Utrecht University

Faculty of Science

Testing the pALPIDE v2 chip for the upgrade of the ALICE Inner Tracking System

Bachelor Thesis

NIKHEF

National Institute for Subatomic Physics

Author:
P.J. Verschuuren

Supervisors:
Dr. Paul Kuijer
Dr. Panos Kristakoglou

Abstract

In the second long shut down of the LHC at CERN scheduled in 2018-19 a big upgrade of the ITS of the ALICE detector is planned. In light of this we discuss what the current state is of our view of the Standard Model, how Quantum Chromodynamics plays a role in it and how the gaps that are still left open can be answered by the study of Quark Gluon Plasma. When the goals in this theoretical view are set we discuss which of these are of interest to the ALICE collaboration, what the current performance and limitation are of the ALICE detector and how the ITS upgrade is going improve the current performance. Among many key aspects of the ITS is the pixel sensor system the most important and for this upgrade the new Monolithic Active Pixel Sensor architecture ALPIDE is chosen because of its best fit with the requirements set by the ALICE collaboration. One of the chips that is used to explore electrical and mechanical testing possibilities is the pALPIDEv2 chip. This chip is embedded on a flex printed circuit for which we developed a cable to connect it with a MOSAIC board. Furthermore was a power grid developed to connect it with a 5V power supply. After connection was made the chip was tested on several important qualities that not only determined how well the tested chip matches the requirements of the ALICE collaboration but also explores the possibilities of future tests. The chip has four distinct pixel areas which are compared on their thresholds, noise and faulty pixels. By extracting the data with a C++ written program further statistical analysis could be performed after developing applicable Root programs. After showing significant differences in threshold, noise and faulty pixels this paper leaves a lot of room for further research i.e. testing this chip or upcoming versions of the ALPIDE-chip in an array.

Contents

1 Introduction **3**
1.1 The Standard Model . . . 3
1.2 Quantum Chromodynamics . . . 4
1.3 Quark Gluon Plasma . . . 5

2 Motivation **6**
2.1 Physical Goal of ALICE . . . 6
2.2 Current Detector Performance and Limitations . . . 7
2.3 ITS Upgrade . . . 9

3 Experimental Setup **11**
3.1 pALPIDE v2 chip . . . 11
3.2 Power Supply and Data Cable . . . 12
3.3 Graphical Interface and Data Read-Out . . . 13
3.4 Root Analysis . . . 14

4 Measurements **16**
4.1 Pixel Map . . . 16
4.2 Threshold Distributions . . . 18
4.3 Noise Distributions . . . 21
4.4 Faulty Pixels . . . 24

5 Conclusions **26**

6 Discussion **27**

A Probabilities of Chi Squared **28**

B FPC connections **29**

C Faulty Fits **32**

1 Introduction

1.1 The Standard Model

The Standard Model is designed to provide a theoretical framework for classifying all the possible elementary particles and the fundamental interactions between them. In this section we will give a short description of the current known particle classes with a summary of their most important properties and briefly describe the workings of the electromagnetic, weak and strong interactions. The follow-up section will provide a deeper understanding of the strong interactions since this is the main goal of the ALICE experiment. The Standard Model has been self-consistent in theory and provided successfully experimental predictions until this day. However, there are still a lot of issues that remain unresolved in the physics of subatomic particles. We will focus on the questions that lay in the scientific scope of the ALICE experiment.

The Standard Model is divided into 2 classes of particles with several subclasses which are all characterized by multiple properties.

Figure 1: The Standard Model[1]

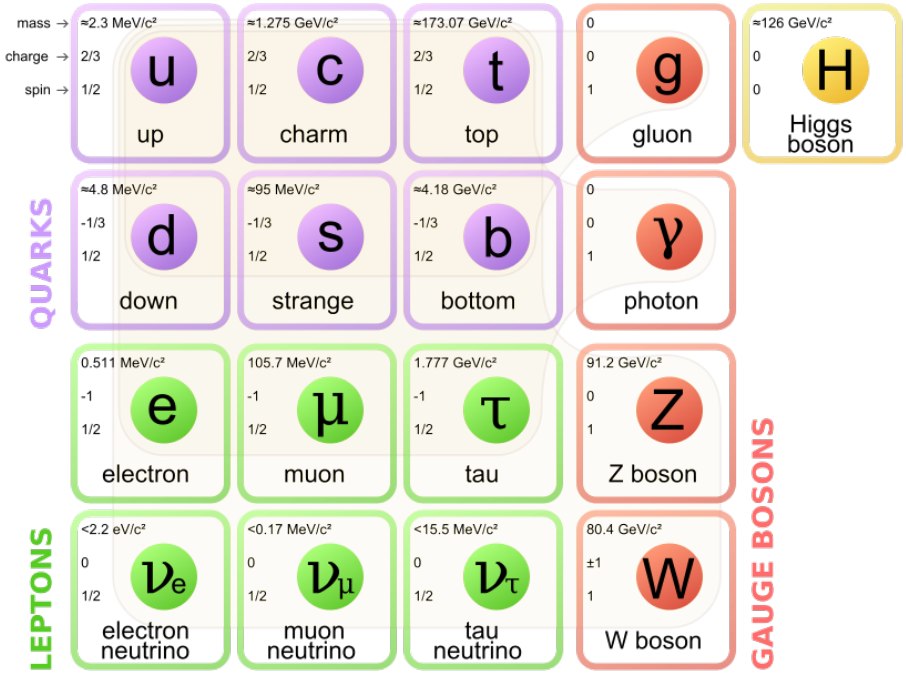

In the figure above a clear schematic is given of the elementary particles in which the first 3 columns make up the class of fermions, which are particles with spin 1/2, and the last 2 columns are called the bosons which have a spin of either 0, 1 or 2. The fermions are the particles that make up all the matter, which all have an antiparticle with opposite sign quantum numbers and can be subdivided into quarks and leptons.[1] The difference between quarks and leptons, besides all the ones given in figure 1, is that quarks and leptons interact differently with each other and them selves. All the fermions can interact via the weak interaction so no distinction there between quarks and leptons. The electromagnetic interaction can only happen between particles with an electric charge so the neutrino's only work via the weak interaction but the electron, muon, tau and quarks all have charge so they do interact electromagnetically. The difference is that the quarks, unlike the other fermions, also have a property called color charge and are therefore the only fermions that can interact via the strong interaction.[1] The physics of the strong interaction is explained in the theory of Quantum Chromodynamics which we will describe more extensively in the next section.

The strong, electromagnetic and the weak interaction all are forces that are mediated by force carriers which in the Standard Model are known as the bosons. The $W^{\pm}$- and the Z^0-bosons are the force carriers for the weak interaction and are together with the Higgs-boson the force carriers with mass. The electromagnetic interaction is mediated through the exchange of virtual photons between particles with charge and is in the order of 10^4 times stronger than the weak interaction. Together these forces can be unified into the electroweak theory.[1] The gluon is the mediator of the strong force that can act between quarks, with itself and is in the order of 10^6 stronger that the weak force. This makes it by far the strongest fundamental force.[2] Lastly, the Higgs boson describes the interaction of the Higgs field with other elementary particles but does not mediate another fundamental force. This is because all the other bosons are associated with gauge symmetries while the Higgs boson plays a role in spontaneous symmetry breaking. Note that the gravitational force is not yet incorporated in this model. There are some speculations that a graviton with spin 2 should be the force carrier for gravitational interaction but such a particle is still to be found.[1] Though there are many other unresolved issues in the Standard Model like the incorporation of dark matter and energy or the asymmetry in matter and antimatter, the biggest questions addressed by ALICE are about the origin of confinement and the generation of mass. Until this day we do not know why quarks are not observed in isolation or why the quarks only make up 1/100 of the total mass of a proton and neutron. In the next section we will explain more about the theory of the interactions between quarks and gluons and how these questions are part of this theory.

1.2 Quantum Chromodynamics

The strong interaction is the force that makes sure that all matter is stable and that protons, neutrons and compositions of the two aren't torn apart by the electromagnetic force. The force is only limited by Pauli's Exclusion Principle and acts mostly in a range between 0.5 and 3 femtometer, the distances between and inside nuclei. This interaction is described by Quantum Chromodynamics, a non-abelian gauge theory part of the general quantum field theory which describes all the elementary particles and their force carriers.[3] All quarks and gluons have color charge which doesn't imply our visible perception of the quarks but are analog to electric charge and the electromagnetic interaction. The color charges can be either (anti-)red, (anti-)green or (anti-)blue and by exchanging one of the eight massless gluons quarks with different color charges can interact. Just like the electromagnetic interaction the gluon mediates the force with the speed of light but unlike the photon it does carry charge and in this case color charge.[4] Unlike the other forces which diminish when distance is increased, the strong force keeps increasing until the force reaches a certain constant value. This creates a potential that is so high that when quarks in confinement are pulled apart new quark-antiquark pairs are created instead of extending the quarks any further.

$$V_{\mathrm{QCD}}(r) = -\frac{4}{3}\frac{\alpha_{\mathrm{s}}}{r} + kr \tag{1}$$

Equation (1) is the potential that is used for the strong force and as you can see with increasing r the first term will eventually be insignificant and the potential will keep increasing linearly until the size of about a hadron is reached and it takes on its constant value.[5] In particle accelerators like ALICE this energy value creates jets of quark-antiquark pairs which is called hadronization and is one of the phenomena that is being studied there. This is the reason why we think that color confinement exists but the strong interaction isn't well known enough to have a clear proof. [8] Another issue is the generation of mass. When the mass of a proton or neutron is compared with the quarks that make up the nuclei the quarks only generate 1% of the mass of the nuclei. It is thought that the strong interaction that confines the quarks in the nuclei also is responsible for the generation of the rest of the mass of matter. Finally, the theory of Quantum Chromodynamics predicts that although quarks are confined that with a very high energy reaction the quarks and gluons no longer will be confined but will reach asymptotic freedom. This is a phase state that is created inside the ALICE experiment during collisions of high energies in the order of TeV and is called a Quark Gluon Plasma. This state is to believed to answer a lot of questions about

the effect of confinement, the generation of mass but also is the state in which the universe was until a few seconds after the Big Bang and plays a role in the inside of neutron stars.[6] The Quark Gluon Plasma is therefore an important phenomenon, a big part of the theory of Quantum Chromodynamics and therefore the Standard Model.

1.3 Quark Gluon Plasma

At the Large Hadron Collider of CERN, heavy ion collisions are generated by accelerating 2 beams of lead ions to an center of mass energy of up to 5 TeV and letting the beams cross each other at multiple experiments like ATLAS, CMS and ofcourse ALICE. These ions are accelerated to a speed near the speed of light and therefore take on the form of a flat disk because of the length contraction stated in the theory of special relativity.[7] When the nuclei inside the ions collide they create a heat that is comparable with temperatures in the order of 5.5×10^{12} degrees Kelvin and generates enough energy to let the nuclei melt into a soup of seemingly free gluons and quarks, collectively called partons.[8]

Figure 2: Quark Gluon Plasma [6]

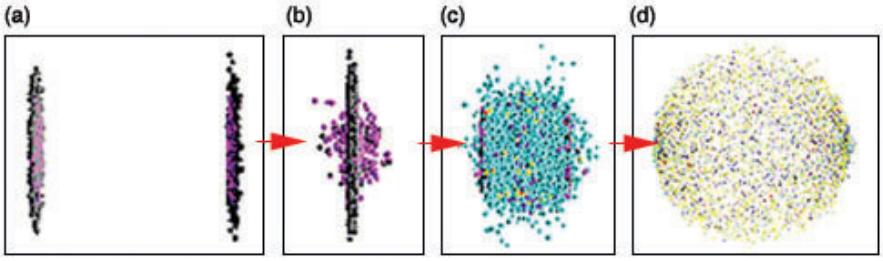

The above figure is a representation of how the collisions take place. What should be noted however is that the disks of nuclei almost never collide so perfectly head-on. The parameter that expresses how "head-on" the collisions are is called centrality where a collision with 0% centrality being a perfectly aligned collision. This is one of the first parameters taken into account and can make a big difference in the retrieved data. Since almost no collisions have 0% centrality a lot of collisions have a part of the nuclei that don't take part in the collisions and pass through unnoticed. The ones that are in the collision plane create a fireball that de-confines the quarks and gluons and make the phase transition to a Quark Gluon Plasma.[9] This phase however only holds very shortly and cools down very quickly which results in recombination of quarks into ordinary matter. This creates a shower of particles with enormous multiplicity among which besides hadrons also photons, muons and dileptons(which are particle anti-particle pairs of the same flavour lepton). These particles and their energies are studied as probes to address multiple characteristics of the QGP. [6] In relation to normal plasma the QGP has some similarities and some differences. Like normal plasma where charges are screened, so are also the color charges screened in a QGP. However, unlike plasma which behaves gas-like, the QGP acts more like a near-perfect Fermi liquid. This gives us a perfect way of studying Quantum Chromodynamics as a multiple-particle theory by looking at this strongly interacting matter and its characteristics in temperature and transport coefficients. Insight in these observables can be found by looking at strangeness production for instance. Strange quarks don't occur in normal matter which is constructed from up- and down-quarks but is created in this case by parton collisions in the QGP. After the hadronization a lot of detected particles will contain strange quarks and thus information about the collisions, dynamics and other conditions of the QGP. The same is thought about heavier quarks like charm and beauty which make the hadrons containing these quarks very interesting for future research.[8] Another important observable is elliptic flow which is a hydrodynamical concept which describes how anisotrope the partons move inside a QGP. Short after the collision a system with large multiplicity, i.e. a large amount of particles, is created in which flow of energy, momentum and particles takes place.

Flow is directly correlated to particle interactions which are indicators of thermalization. Therefore, especially in the early stages, elliptic flow can tell how the thermalization takes place and on what time-scale.[12] Now that we have our broad theoretical view of the ALICE experiment we will take a closer look at the goals of ALICE within the issues that were briefly discussed in the previous sections.

2 Motivation

2.1 Physical Goal of ALICE

The overall goal of ALICE is to fill in the theoretical and experimental gaps that are still unanswered in the Standard Model and Quantum Chromodynamics by studying all the phenomena that occur at proton-proton, proton-lead and lead-lead collisions. The most interesting and foremost important phenomenon is the strongly interacting matter phase of the Quark Gluon Plasma. Thus by looking at the observables that clearly show the dynamics and constituents of the QGP the ALICE collaboration hopes to achieve this goal. Because there are too many observables to discuss in this thesis we will begin with the two phenomena that are important for the goal of understanding of the QGP but also have some unexplored areas which will be ventured with the upcoming upgrade.

Thermalisation and Hadronisation
When the Quark Gluon Plasma is created a multi-particle system arrises which evolves and tries to find equilibrium. This process is called thermalization and by looking at the number of interactions and the emerging particle velocities one can state how close the system is to equilibrium.[8] The number of interactions between partons can be measured by looking at the heavy flavour hadrons that emerge from the interactions.[11]

Figure 3: The process of determining parton interactions[13]

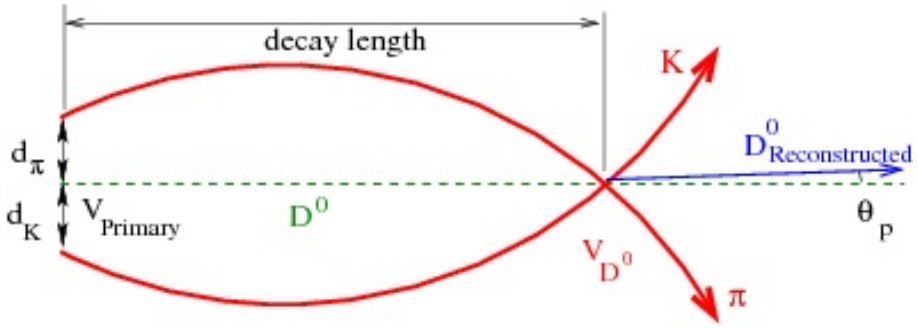

Because heavy flavor hadrons(e.g. D_0-mesons) have a very short decay length such that the primary interaction(i.e. vertex) must be determined by the tracks of the decay product(e.g. kaons and pions). This way the track of heavy flavor hadrons can be reconstructed with a margin θ_p also known as the impact parameter. Also the velocities of the emerging particles can be measured with this model and the collective flow of the medium along with it. In this collective flow we make a distinction between the radial flow and anisotropic flow.[10] The radial flow states the shared radial expansion of the partons and the anisotropic flow states the spatial distribution of the expansion. By looking at the ratio between the flow of particles in the y-axis and the flow of particles in the reaction-x-z-plane the elliptic flow also known as the second Fourier coefficient v_2.[12]

Energy Loss and Mass Dependence
Besides the flow of particles it is also important to know the flow of energy and momentum where we again focus on the heavy flavour quarks. Energy loss of partons and heavy quarks inside the QGP can be characterized by the mass of the hadrons they produce. When a medium through which the partons and quarks move is more dense the partons and quarks lose more energy and therefore momentum.[11]

Figure 4: Flow illustration of a heavy ion collision[14]

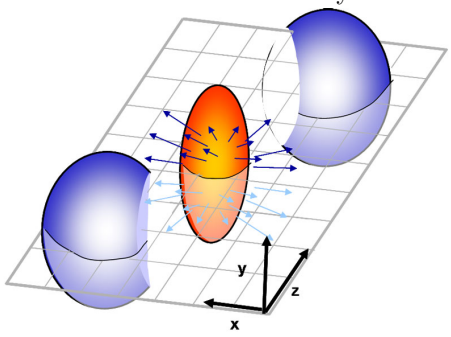

This creates a surppression of detected high energy hadrons when QGP is created and thus a higher count of high energy hadrons with less dense systems. Because of this phenomenon the ratio between the numbers of a certain hadron created with Pb-Pb collisions and p-p collisions gives another important observable R_{AA} also known as the nuclear modification factor. By looking at different heavy flavor hadrons (e.g. D- or B-mesons) at a wide transverse momentum range one can study the energy loss and its mass dependence by looking at the nuclear modification factor.[11]

2.2 Current Detector Performance and Limitations

Now that we know what the important observables are for the goals of the ALICE collaboration we will discuss the current detector, how it measures these observables, how it is performing and in what way its limitations interfere with its previous mentioned goals. Even though a lot of sub detectors are visible in the illustration below we will not discuss them all. Because of the complexity of the ALICE detector we will mostly only discuss the performance and limitations of the most inner sub-detector, the Inner Tracking System (ITS).

Figure 5: Schematic illustration of the ALICE detector[7]

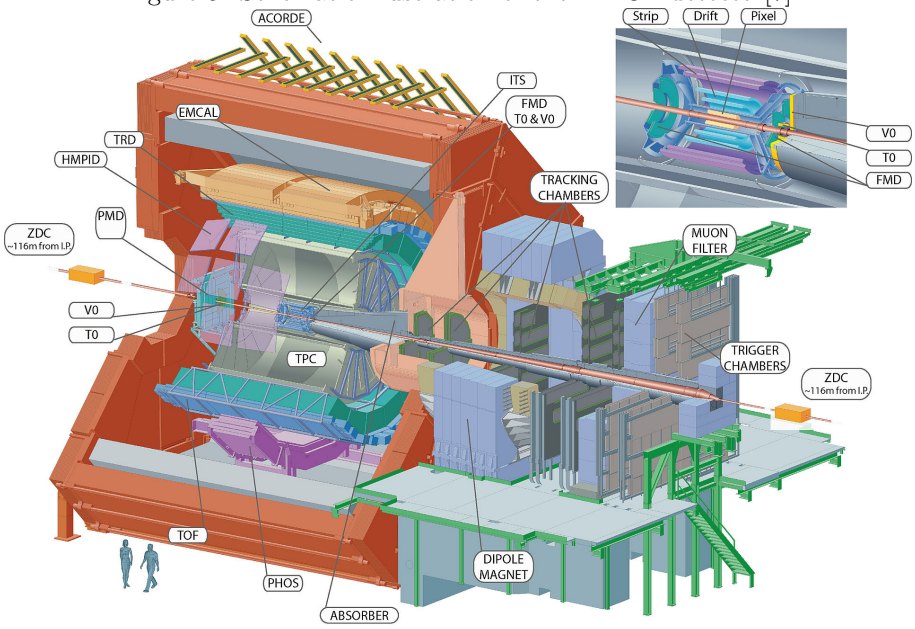

The ALICE detector was first designed and constructed in 1993 from which in the following years a lot of sub detectors were added. All of the sub detectors have their own specific purpose regarding which observables of which particles and on what kind of information from previous detectors

they already rely. As one might guess, the outer detectors mostly rely on the information of the inner detectors and therefore is the information that the Inner Tracking System gathers not only important for its own specific scientific analysis but also for the other detectors such as the Time Projection Chamber or the Time of Flight detector. The TPC can then calculate the velocity for instance, just like the TOF detector but then with a different technique, while the other calorimeters calculate the energy of the particles and determine if they interact hadronic or electromagnetic.[7] By gathering and integrating the information of all the detectors ALICE can identify the particles emerging from the QGP and thus study the properties of the QGP.

Inner Tracking System (ITS)
The function of the ITS is to determine the location of passing and therefore vertices of the particles as precise as possible. The ITS is thusly designed to optimize track finding and create the highest possible impact parameter resolution. For this reason it lies as close as possible to the collision point consisting out of 6 cylindrical layers of silicon detectors:

- 2 layers of SPD (Silicon Pixel Detectors)
- 2 layers of SDD (Silicon Drift Detectors)
- 2 layers of SSD (Silicon Strip Detectors)

The SPD's were chosen closest to the beam pipe because of their high pixels per surface count. The SPD's in the other 4 layers however have some differences. Both the SDD's as well as the SSD's have analogue read-out and are double layered which make them a lot thicker in material. The higher amount of material reduces the tracking performance a lot. With a track density of up to 80 per cm^{-2} in the inner 2 layers and 1 per cm^{-2} in the outer 2 layers it is understandable for the inner layers need better spatial resolution[15] but all over it is still needed to increase the pixel density with factor of 50.[11] Especially in the low p_T region is the impact parameter resolution does not live up to the expectations of the collaboration. Even the Silicon Drift en Silicon Strip Detectors also function as a spectrometer by identifying particles with their dE/dx, i.e. energy loss, in the non-relativistic p_T region have a certain p_T cut-off. Not only for these but for all the observables that are important for ALICE is the low p_T region a problem area. Lastly, it should be noted that a big limitation of the current ITS is the read-out rate.

Current ITS[11]:

Detector	R/O time (μs)	Max. rate (Hz)
SPD	296	3300
SDD	1023	985
SSD	310	3265

The above read out rates depend on the dead time, the minimum time a pixel needs between two successive hits to "reset" itself. The maximum rates are therefore in case that this dead time is 0 which of course in reality is not the case. Since the upgrade of the LHC in the long shut down of 2013-15 center of mass energies are reached of up to $\sqrt{s}$=5.5 TeV for Pb-Pb collisions and $\sqrt{s}$=14TeV for p-p collisions. These kinds of energies give a particle rate of 50 kHz for the Pb-Pb collisions and over 350 kHz for the p-p collisions, i.e. a lot higher than the maximum rates that can be handled by the silicon detectors in the current ITS.[16]Furthermore, each year a shut down is planned for maintenance and repair of the detectors of the experiments at the LHC. This short window has to be used optimally to keep the performance of all the sub-detectors of ALICE up-to-date. Especially for updates on the high data infrastructure the ALICE detector is very inaccessible which makes quick accessibility a large flaw in the current design.[17] Lastly, one should take into account the current integration time of the silicon detectors. The integration time is the minimum time a detector needs to be read out. This thus represents the sensitivity of the detector in which the smaller the time window needed, the better the event reconstruction and analysis. The current integration times, $> 20\mu$s, along with the expected interaction rates imply a significant pile-up of data which again creates a big read-out bottleneck.[11]

We can see that even though the ITS has a clear goal and uses a lot of the right techniques and instruments, it still needs a lot of improvements on several areas. We have seen that this is mostly the case with the tracking efficiency in the low p_T region, impact resolution for determining of vertices and readout capabilities.

2.3 ITS Upgrade

As we saw in the previous section there are some clear limitations present with the current Inner Tracking System. However, during the upcoming Long Shut Down 2 planned in 2018-19[19] the whole ALICE detector will undergo a huge upgrade with ITS being a important part of that upgrade. This will push the boundaries and limitations given in the previous sections even further.

First of all we will discuss some structure modifications. In the picture below you can see a schematic view of what the upgraded ITS is going to look like.

Figure 6: Upgraded Inner Tracking System[17]

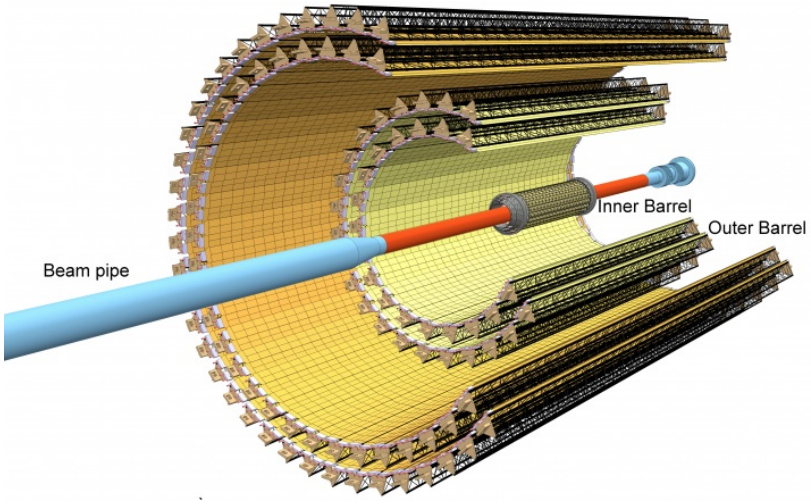

First of all, as one might see is that instead of 6 the upgraded ITS will have 7 cylindrical layers and instead of a mix of SPD's, SDD's and SSD's all the 7 layers will be made of Silicon Pixel Detectors. The ALICE collaboration determined that if the upgraded ITS would keep its PID capabilities the contribution would be to small. But because the amplitude of the particle signal is no longer read-out the whole ITS is read-out binary instead of partially analogue.[19] This makes a great overall read-out speed en precision improvement and a decrease in power consumption. Furthermore, the most inner layer has been placed closer to the beam line by moving from a radius of 29 mm to 17.2 mm.[18] This is one of the steps taken to improve the impact parameter resolution for the heavy flavor quark measurements. All the layers of Silicon Pixel Detectors consist out of the following components:

- **Space Frame:** A light weight carbon fiber support structure
- **Cold Plate:** Another carbon fiber structure for embedding of the cooling pipes
- **Integrated Circuit:** A flex printed circuit on which the pixel chips are bonded

All these structures have their characteristics but the most important element of the ITS is the pixel chip uses as tracking devices in the Silicon Pixel Detectors. The sensors that are the best fit for the goals and demands of ALICE are the Monolithic Active Pixels Detector (MAPS). When a charged particle passes through the medium of a pixel it knocks a lot of electrons out of their place and creates electron-hole pairs in the medium. The electron-hole pairs are pulled apart by the electrical field that is applied on the pixel and accumulates charge on opposite sides of the pixel which creates a electrical current i.e. a signal. This is a simplified model but it is the general

process of how a particle is detected by MAPS.[20] These particle sensors and their corresponding read-out electronics determine how efficient the ITS can identify vertices and tracks of the particles and carry therefore many demands when regarding pixel density, material thickness, power consumption, radiation hardness and read-out speed.[21] By decreasing the pixel size one can increase the pixel density and by doing this hopefully a impact parameter resolution of 5 μm for the inner barrel and 10 μm for the outer barrel is reached. Decreasing the material thickness ensures that the budgetary demands are met though this also puts a constraint on power consumption and more specific the power density possible on a sensor. Furthermore, the detection efficiency has to be at least 99% and the fake hit rate of a sensor needs to be below 10^{-5} to ensure that data loss is minimized.[20] These are several of the demands which the MAPS-chips have to meet and to meet these requirements several R&D groups simultaneously developed different MAPS-chip architectures. Of all the different architectures the one that was deemed best by the ALICE collaboration and which is currently further developed to eventually take its place in the ITS upgrade is the ALPIDE chip.

The ALPIDE and pALPIDE chip

In the beginning of R&D for the new MAPS-chip the architectures in question where MISTRAL, ASTRAL, CHERWELL and ALPIDE. With all different electrical and mechanical properties they were used to test which structures and systems were the best for which purposes. Eventually the ALPIDE chip was chosen because of several characteristics which fit the upgrade demands best.

The ALPIDE pixels will all have their own built-in pixel memory which can either contain a 0 when it is not hit or a 1 when it is hit. Furthermore is the read-out of the pixel memories triggered by hits thus resulting in quick and responsive pixel read-out of hit pixels and power reduction by the non-hit pixels since they do not require a signal.[17] Another important feature is that it has a low integration time, which is the minimal time for a pixel to reset after a hit, to ensure that the high particle rate in the order of 200kHz can be managed. Furthermore has the pixel size decreased to one of the smallest sizes possible making a total of over 5×10^5 pixels per chip to ensure high resolution.[18]

ALPIDE-chip[17]:

Pixel Size (μm^2)	Integration Time (μs)	Power Consumption (mW cm^{-2})
28x28	4	< 50

But as always the road to the actual goal takes a lot of tests and to undergo these tests the pALPIDE chips are used to explore electrical and mechanical possibilities for the eventually used ALPIDE. But besides tests to determine the best possible architecture of the ALPIDE chip the pALPIDE chips are also used to develop a quality insurance check. By testing enough pALPIDE chips to make a statistical sample of chip qualities on certain aspects the ALPIDE chips can be categorized in quality groups. In this way a benchmark is created and the chips with the best functional performance and geometrical requirements can be used to be mounted on the modules which will be used for the ITS. The ALPIDE chips are made at Towerjazz, a integrated circuits manufacturer which pushes the boundaries of its camera pixel detector chips to build chips for the ITS. Because the requests of ALICE are so demanding the standard yield of 95% normally met by Towerjazz is lowered to ±60%.[9] Thus to increase the production efficiency the best pALPIDE chips are picked out to use for duplication in the development process. This way a better yield can be achieved when production of the actual chip is initiated. We saw that in light of the research of ALICE the Inner Tracking System has very specific goals which are not achieved because of certain flaws and limitations in the current design. The purpose of our research was to test the pALPIDE v2 chip on possible mechanical and electrical setups, develop functionality tests and to determine with these tests if this chip would meet the requirements set by the ALICE collaboration. By determining which experimental setups and functional tests are possible we hope to give a handle for all future tests of the pALPIDE chips and of course the ALPIDE chip for fast setup and research start. By testing the current pALPIDEv2 chip we can give an overview on which requirements are met, on which there should be improvements and which characteristics need further looking in to.

3 Experimental Setup

3.1 pALPIDE v2 chip

The pALPIDE v2 chip is a MAPS with a pixel matrix of 512 double columns and 512 rows organized in 32 regions which are read-out parallel. The whole matrix is further divided into 4 equally sized but differently characterized sub-matrices e.g. with differences in noise-to-signal ratio. Each pixel has a threshold that can be set and which determines what the minimum passing charge should be for the pixel to be hit.[22] This can be done by a particle beam but also with a chip build-in injection signal to simulate the passing of a charged particle.

Figure 7: Pixel Schematic

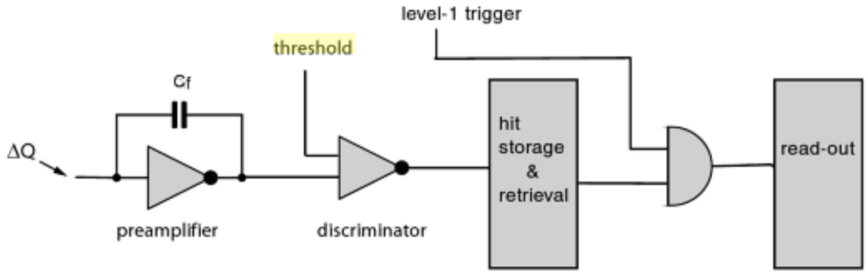

The above figure is a schematic of the hit, register and read-out functionals. When the signal ΔQ comes in, be it from an injection or a external particle, it first gets amplified and send to the discriminator for comparison with the set threshold. Then it gets stored in the register of the pixel and eventually read-out when triggered. Setting the threshold, injecting a charge signal and read-out is all controlled by the flexible integrated circuit on which the chip is embedded. We will give a short summary of the pALPIDEv2 chip interface and which signals are needed to control the process stated above.[22]

The first signal that should be taken into account is CLK also known as the clock signal. This is the master clock along which all the processes are synchronized in timing. In this case it is a 40 MHz oscillator which regulates all the digital circuits of the chip. Another function of this signal is suspending all the operations and readouts on the chip by stopping the signal all together. Secondly, there is the CNTR which gives full access to the control and status registers of the chip. This simply gives control over all interfaces of the chip and the flex printed circuit. Lastly, the DATA signal functions as data output signal for all the readouts performed by the user.[22]

Figure 8: pALPIDE Chip Pads[22]

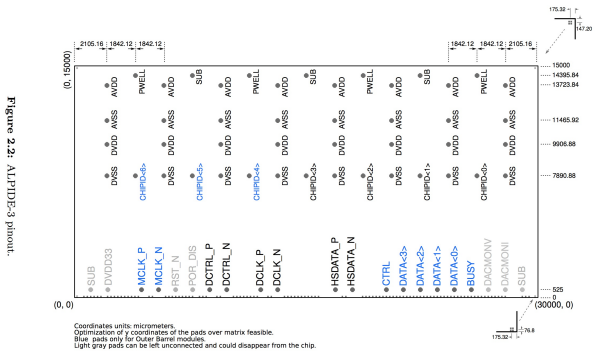

Figure 2.2: ALPIDE-3 pinout.

The figure on the previous page gives an oversight of where all the signals can be found on the flex printed circuit. We used this to connect the right chip pads so that we know which signals are transmitted through which cable line and to which I/O-pin. This way all the above mentioned signals can be connected to the right I/O-pinout addresses to ensure control over the chip. In Appendix B one can find photos of actual chip pad connections to give a good visual guide for future research.

3.2 Power Supply and Data Cable

Power Supply
Supplying the pALPIDE chip with power needs to done with caution to ensure that no damage to the chip is done. The power grid is build to convert the power of the Nikhef power supply to the right voltage and ampere but also to ensure that the chip is guarded from wrong power settings and connections.

Figure 9: Schematic Power Grid[23]

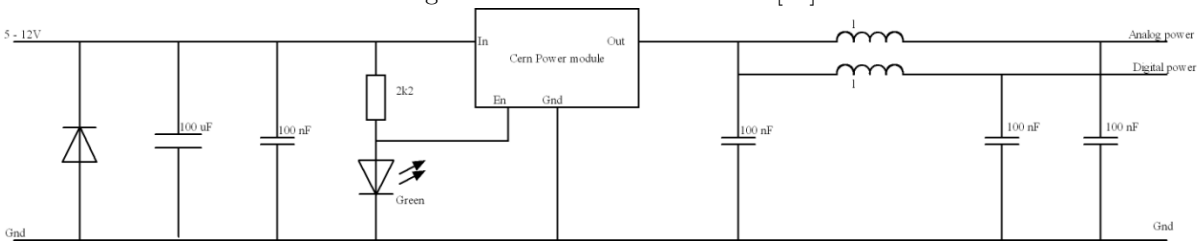

Figure 10: Detailed Power Grid

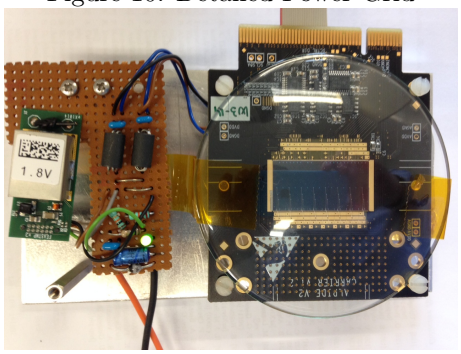

The two pictures depicted above are the schematic and detailed pictures of the intermediate power grid which had to be developed to make sure that the 5V power supply gave the right output to the power module of the chip. On the most left is a diode which ensures that the switching of the poles won't damage the chip when current is running backwards through the circuits of the chip. The green emitting diode functions as on-light and as an 1.8 voltage limit for the En_entrance which can only take 3.3 volt.[23] The capacitors are used to filter high and low frequency interference and furthermore there is a security diode implemented to make sure that the circuit is secured in case of a sudden switch of power supply polarity. The electrical resistance is placed to keep the voltage through the diode limited and the coils are there to split the power signal into a analog and digital part. In combination with the coils and high frequency capacitor this diminishes the interference with a factor of 5000 thus ensuring a clear power signal.[23]

Data Cable
As indicated before the purpose of the data cable is to regulate the I/O of the pALPIDEv2 chip via the flexible printed circuit on which is mounted. The 3 signals that are needed for the regulation are CLK, CNTR and DATA which are all Low-Voltage Differential Signaling(LVDS) signals. This is a double wire connection with 100Ω at the end and the signal differentiates between 1 and 1.4 V. Differential send signals have the advantage to be less sensitive for common-mode noise so that the signals send through lose less information.[23]

Figure 11: The overall experimental setup

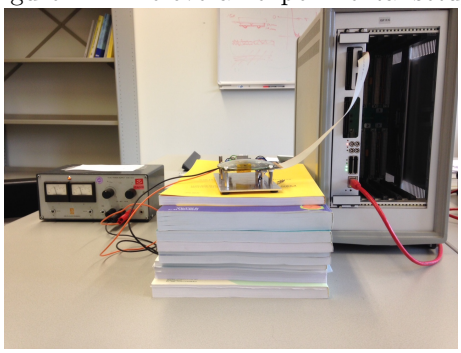

The above picture clearly depicts the setup of the power supply, connected to the power grid, the pALPIDE chip and FPC interface which was connected to the MOSAIC board mounted in a back plate. This LVDS cable previously discussed put the I/O through via a FMC port on the MOSAIC board which on its turn was connected via a internet cable with a computer. In this way with pre-written code from a research group from Italy data could be extracted. The MOSAIC-board is a module which is especially designed for the readout and testing of particle detectors. It has several I/O-ports which makes it very adaptable and ethernet connection through which runs control of the operations and data but also makes updates on the firmware possible.[22] This makes it the perfect module for us to fucntion as a mediator between the pALPIDE chip and computer.

3.3 Graphical Interface and Data Read-Out

Besides exploring the properties of the pALPIDE chip and testing them on different levels there was also the need for a graphical user interface for future easy and quick quality tests. This was developed by another member of our research group and made sure that all the important parameters can be set and overall performance view can be given in a user friendly way. We will give a overview of the program, how it works and what form of data it extracts.

Registertest
One of the first tests that can be done with the software is the register test. Each matrix is sub divided into 8 regions of which each region has its own memory register. When a pixel is hit its signal is stored in the register which can be read out to extract the data. The register test sets a certain binary value in the registers, reads it out and compares what comes out with what was originally set. If something different comes out, the register is faulty and the interface will give a red filling to the box which represents the register in question. If the output resembles the input however, the box filling will be green. This is a basic functionality test that is needed for all future chip testing.

Figure 12: Software Register Test

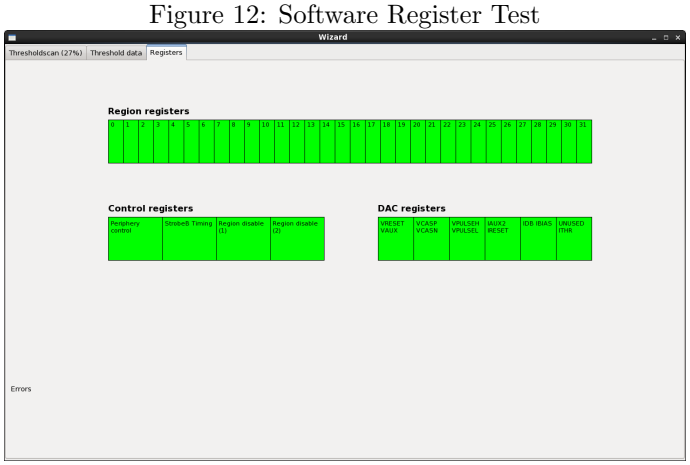

Dashboard
The dashboard is an easy and quick interface of roughly determining the threshold and noise of a pALPIDE chip. Several parameters can be set to the users liking and after running the test it shows the number of pixels tested, the amount of measurements per pixel and the threshold/noise distribution. Furthermore can it export the data for further in depth analysis. Below is a pictorial example of the software.

Figure 13: Dashboard

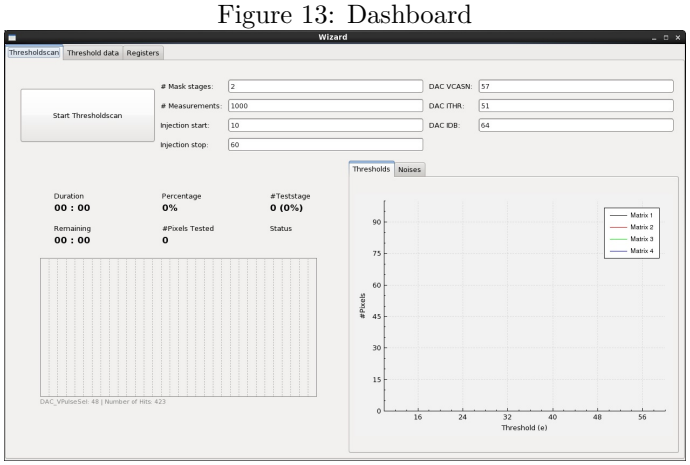

Special thanks goes to Lukas Arts with which this research was conducted. The software that is depicted is designed by him and in co-operation with him we worked out the workings of the chip, how we could make connection and how the tests could be run to extract data for further analysis.

3.4 Root Analysis

After the extraction of the data we used the C++ based software framework called Root to analyze and visualize the data sets. Root is a specialized scientific software framework used to process, analyze, visualize and store big data sets. We first tried to handle the data of the ALPIDE chip with Wolfram Mathematica but with datasets containing more than 2 $\times 10^5$ lines we noticed that Mathematica is not the most time efficient program. We developed several pieces of code in C++ that could be executed by Root to see which pixels exactly were tested, were their thresholds lies and what their noises were. Before we show what the results are we will walk you through the kind of tests, how they were developed and what they can say about the tested pixels.

Threshold and Noise

The purpose of the threshold scan is to determine the signal threshold that is needed for a pixel to be hit. The threshold can either be in units of voltage or if the signal is calibrated it can also easily be converted to charge.[9] When the chips are mounted in the ITS they will be calibrated to charge but since we test with a injection signal we simply use a build-in 8bit Digital-Analogue Converter(DAC) to vary the injection signal. This gives us a range of 256 steps in 1.8 voltage that we have set on our power grid.[24] The threshold which is to be determined can be roughly set by adjusting the parameters on the dashboard of the developed software. By increasing the DAC ITHR and DAC IDB one can increase the threshold and vice versa. By increasing the DAC VCASN however the effect is inverted and the threshold is decreased. These parameters have the following standard setting:

Software Parameters:

VCASN	ITHR	IDB
57	51	64

Figure 14: Thresholdscan and derivative

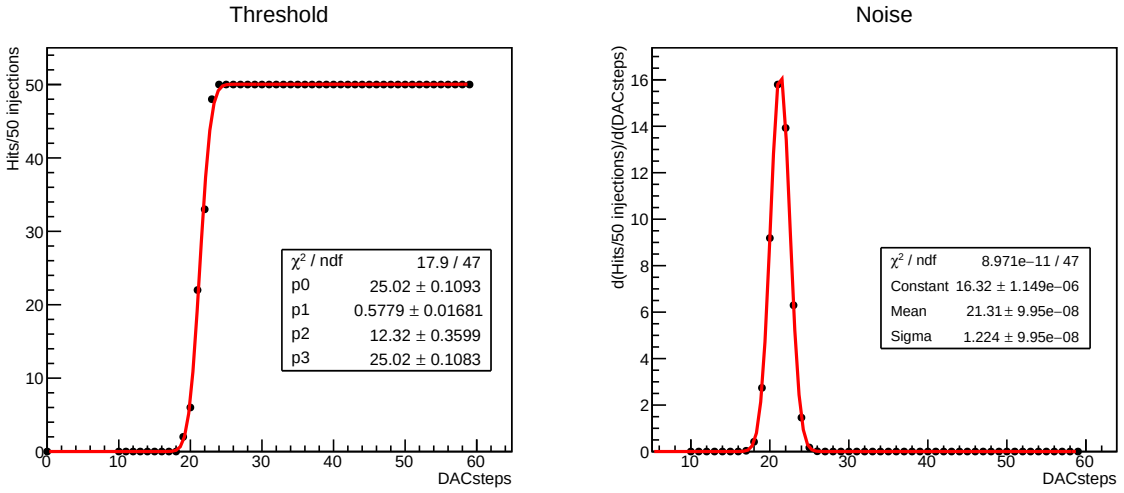

This is a threshold test of a random pixel. In this case we used 50 injections per DAC step to see how many times of those injections the pixel registered a hit. In this case clearly after DACstep 21 the threshold is surpassed and quickly all the 50 injections give a registered hit. These data points are fitted to the error function[15].

$$erf(x) = \frac{2}{\sqrt{\pi}} \int_0^x e^{-t^2} \, \mathrm{d}t. \tag{2}$$

By trial and error the right parameters and their starting points were found to fit almost every all datasets. The reason why the threshold test is not a perfect Heaviside function is because electrical circuits come with noise. These are fluctuations in electrical signals that can be produced by random external influences like thermal fluctuations in the conductor or interference of electromagnetic waves.[9] Some noise however is dependent on the construction, material or imperfections of the electrical device in question or in this case, the pixel in question. By taking the derivative of the error function fit we get again a set of data points which we can fit but this time to a Gaussian function. The mean in this case being the determined threshold and the sigma representing the noise of the pixel. This way we can determine not only what the threshold is but also how noisy a pixel is. This was merely an example to show how we determined the thresholds and noises. In the next section we will show how these quantities are actually distributed over the entire pALPIDE chip.

4 Measurements

Determining the threshold and noise of one pixel in a matrix of more than 2×10^5 pixels is of course trivial. Therefore we extracted three datasets which contained threshold tests of a much higher count.

ALPIDE-chip

	# tested pixels	# test injections	VCASN
Dataset 1	522	50	51
Dataset 2	4096	1000	51
Dataset 3	4096	1000	71

As you can see not all pixels of the chip have been tested as that would require a lot more computing power. Because these tests have to be universally used the pixels are chosen by an algorithm which homogeneously chooses pixels of the pALPIDE chip. The specifics of the algorithm are not important but we can give you a visual aid.

4.1 Pixel Map

To give an idea which and in what order the pixels in the matrix are tested we have constructed a map of the tested pixels for the first and second data set.

Figure 15: Dataset 1

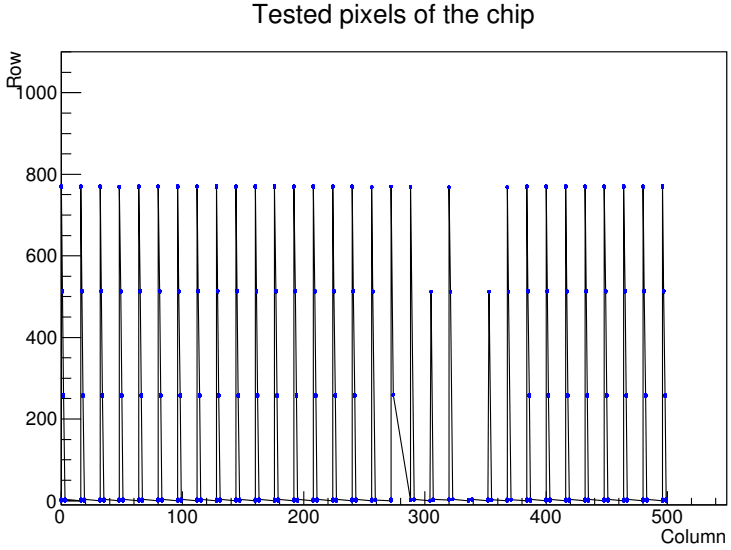

Note: Each blue dot represents 4 tested pixels. Because of the high resolution of the pixel matrix this is badly showable.

One can clearly see that the pattern crosses the chip homogeneously. Furthermore, though the high resolution of the pixel matrix makes it difficult to see, the pattern does run without testing a pixel double. In the first pixel map we can also see that something went wrong in the process of testing or data storage. In upcoming sections we will see what the consequents are for these "faulty columns". The interconnecting lines show in what order the pixels are tested. Especially in the first pixel map you can see that the threshold tests starts in column and pixel number 0, then tests the 3 successive pixel numbers and goes up to pixel number 768. Again after that 3 successive pixel numbers are read out in that column before it switches. This should give an idea of the pattern the threshold test uses to pick the pixels.

Figure 16: Dataset 2

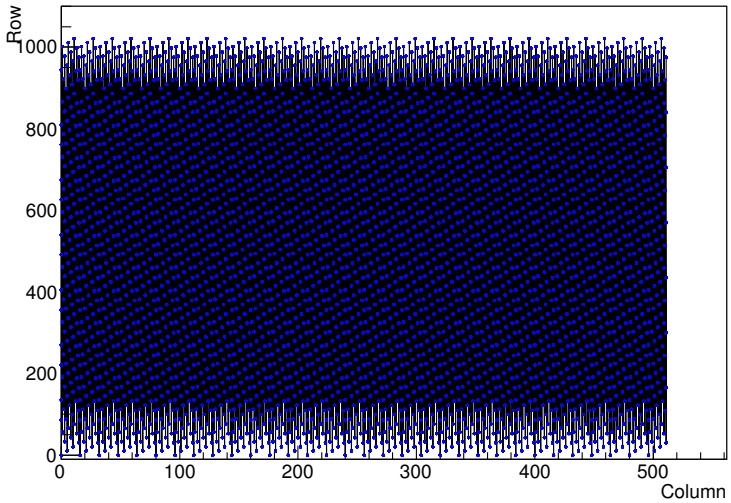

Again this map shows that when increasing the amount of tested pixels they are still homogeneously chosen and ensures no double tested pixels. The pixel map of the third data set is identical to the one of the second data set because the algorithm which chooses the pixels only depends on the number of pixels which is set at the beginning of testing.

4.2 Threshold Distributions

Dataset 1
We start with the first dataset. This is the smallest dataset which is illustrated in the first pixel map in the previous sections. On each pixel a threshold test is run and the noise is determined according to the process discussed in the previous section. Each threshold and noise is put into a histogram and drawn on a canvas.

Figure 17: Dataset 1

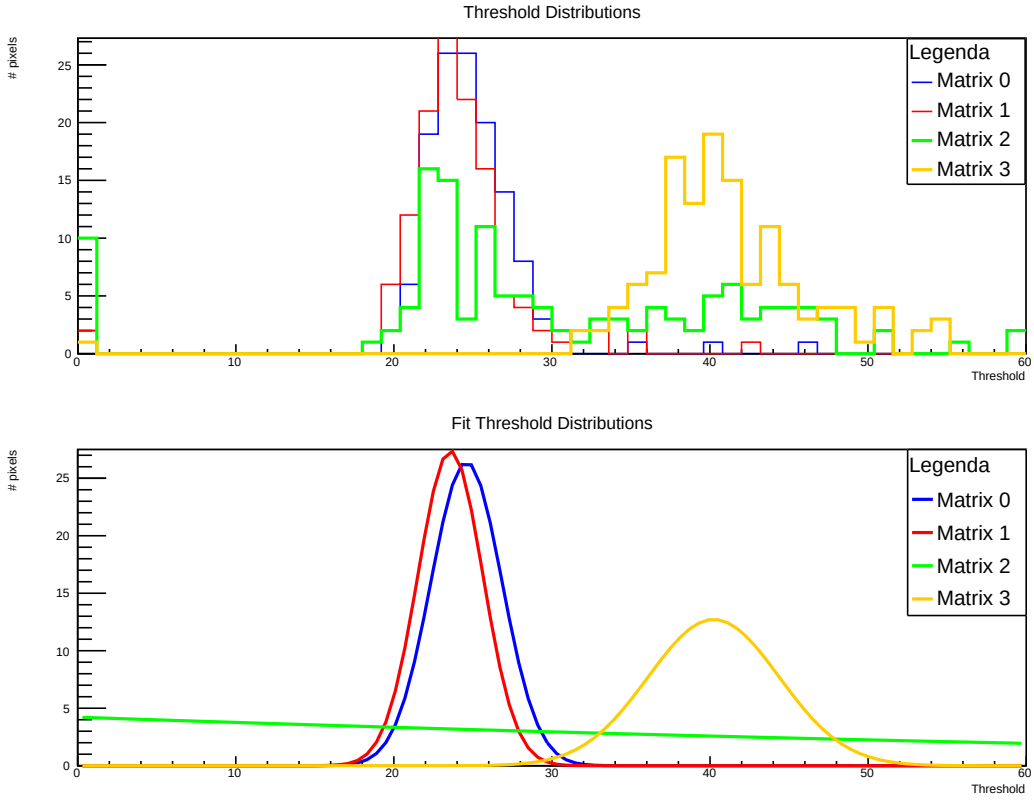

As we can see the threshold distributions of the four different matrices are represented in the above canvas with the Gaussian fits following. One of the most clear characterizations of this data set is that matrix 2 has a much larger spread in the distribution of thresholds which results in a highly ineffective fit. Just like the other 3 matrices should also matrix 2 be a Gaussian fit but the data produces a fit with a very large sigma. Furthermore can a fit have his reduced chi-squared calculated and with this the probability to acquire such a reduced chi-squared or larger if it is assumed that the correct fit is chosen. If this probability is large then the observed and expected distribution is consistent.

Matrix	χ^2	ndf	χ^2/ndf	Prob(χ^2/ndf $\geq$ ${\chi_0}^2$/ndf)	Mean Threshold
0	8.13	11	0.74	$83\% > P > 64\%$	24.6
1	12.83	13	0.98	$66\% > P > 45\%$	23.6
2	48.46	26	1.86	$5\% > P$	-174.5
3	21.60	17	1.27	$25\% > P > 12\%$	40.2

The probabilities were taken from a table in Appendix A. As we can see almost all the probabilities are very large which indicates a good agreement of the fit with the measurements. We do see however that the fit of matrix 2 is by far the Gaussian fit that we would like it to be when compared to the other distributions. When we look at the histogram we see to much spread and when we look back to the pixel map in the previous section we see that matrix 2 has a lot of pixels missing. Not that missing pixels on itself should disturb the distribution but the lack of pixels indicates that something went wrong or very different in matrix 2 then in the other three matrices. We will later look at some "faulty" pixels to see if this regional failure is consistent.

Dataset 2
The first important difference between the previous data set and this one is that the measurements per DACstep per pixel is much higher, i.e. 1000 measurements instead of 50. Secondly our distributions consist out of 4096 tested pixels in stead of 522. The rest of the parameters are the same however.

Figure 18: Dataset 2

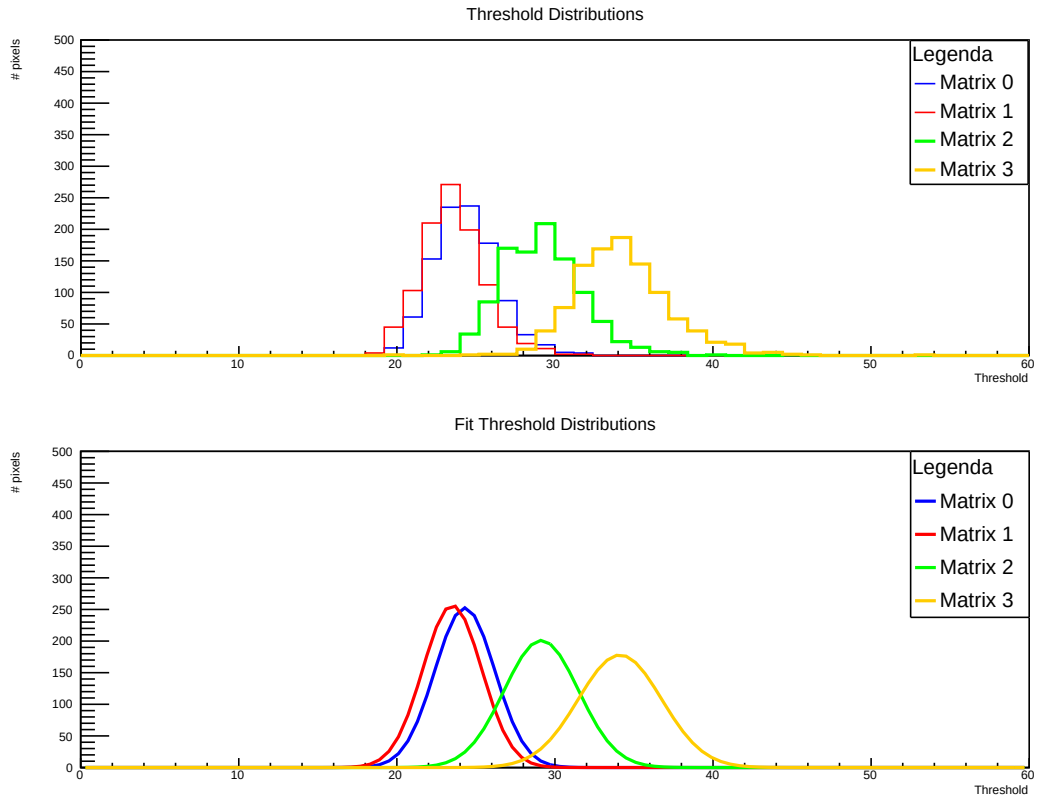

Matrix	χ^2	ndf	χ^2/ndf	Prob(χ^2/ndf $\geq {\chi_0}^2$/ndf)	Mean Threshold
0	21.36	10	2.14	$5\% > P$	24.3
1	24.40	10	2.44	$5\% > P$	23.5
2	34.53	13	2.66	$5\% > P$	29.1
3	42.81	18	2.38	$5\% > P$	34.1

Again we can see that the first two matrices stand out from the last two but with a obvious difference. The distributions seem to have centered themselves much more nicely around a certain mean and matrix 2 does not seem to have the defect that it had in the previous dataset. One should also notice that the distribution no longer can be deemed Gaussian since the probability of the reduced chi squared is below the 5% significance level.

Dataset 3
These are the same pixels tested as the previous dataset though with a heightened VCASN, i.e. a lower threshold. Again however a dataset with a 1000 measurements per DACstep per pixel, 4096 instead of 522 tested pixels and with the parameters ITHR and IDB the same.

Figure 19: Dataset 3

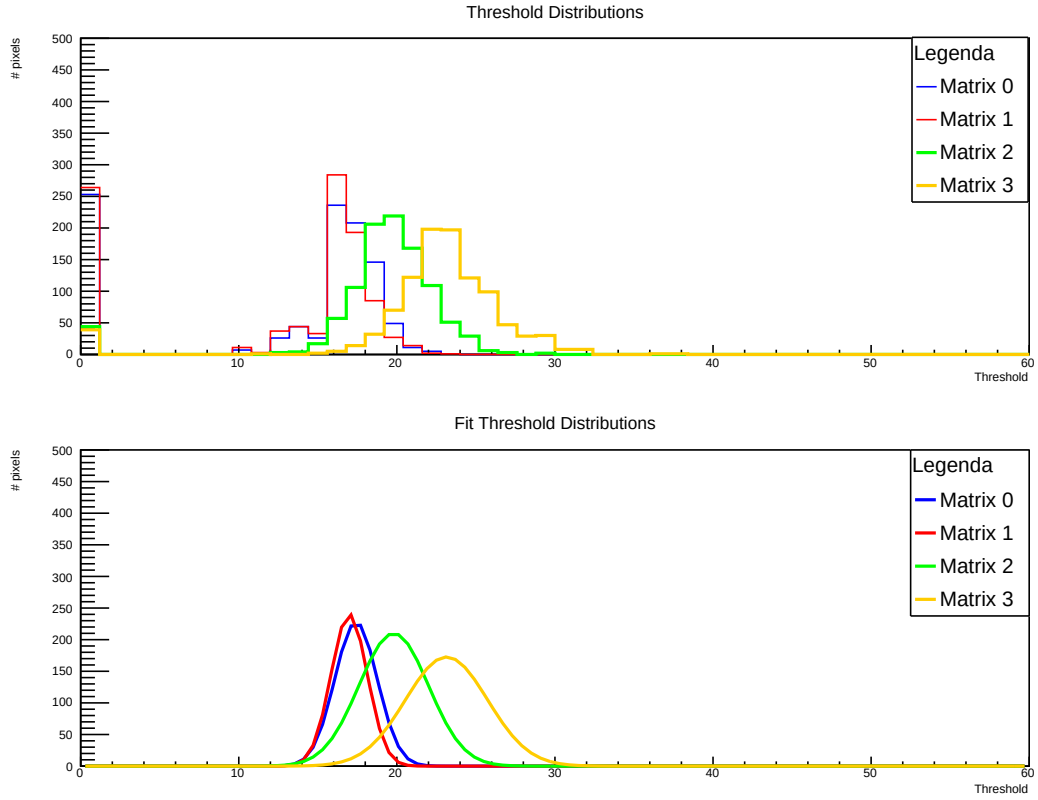

Again several differences can be seen in the distributions and fits. In this case the distribution of matrix 0 and matrix 1 have worsened because of the higher threshold count in the first bin. These could indicate faulty pixels or wrong fits which we will discuss in the next section. We do see that the VCASN heightened gives a clear collectively lowered threshold but what also should be noticed is that the relative distance of the mean thresholds has also been lowered in comparison to the previous mean thresholds. Furthermore, do we see that the reduced chi squared probability has plummeted even further which indicates an even worse Gaussian fit agreement. This could however be explained by the high count of thresholds in the first bin of the distribution which is clearly a unusual high one for matrices 0 and 1.

Matrix	χ^2	ndf	χ^2/ndf	Prob(χ^2/ndf $\geq {\chi_0}^2$/ndf)	Mean Threshold
0	376.06	12	31.34	$0.05\% > P$	17.4
1	424.19	11	38.56	$0.05\% > P$	17.0
2	58.74	12	4.89	$0.05\% > P$	19.8
3	86.20	16	5.39	$0.05\% > P$	23.1

4.3 Noise Distributions

Dataset 1

We have shown in the previous section how the thresholds are distributed, how their fits look like, what differences in their two visualizations looked conspicuous and what they might imply. We will do the same with the noise distributions of the 3 datasets.

Figure 20: Dataset 1

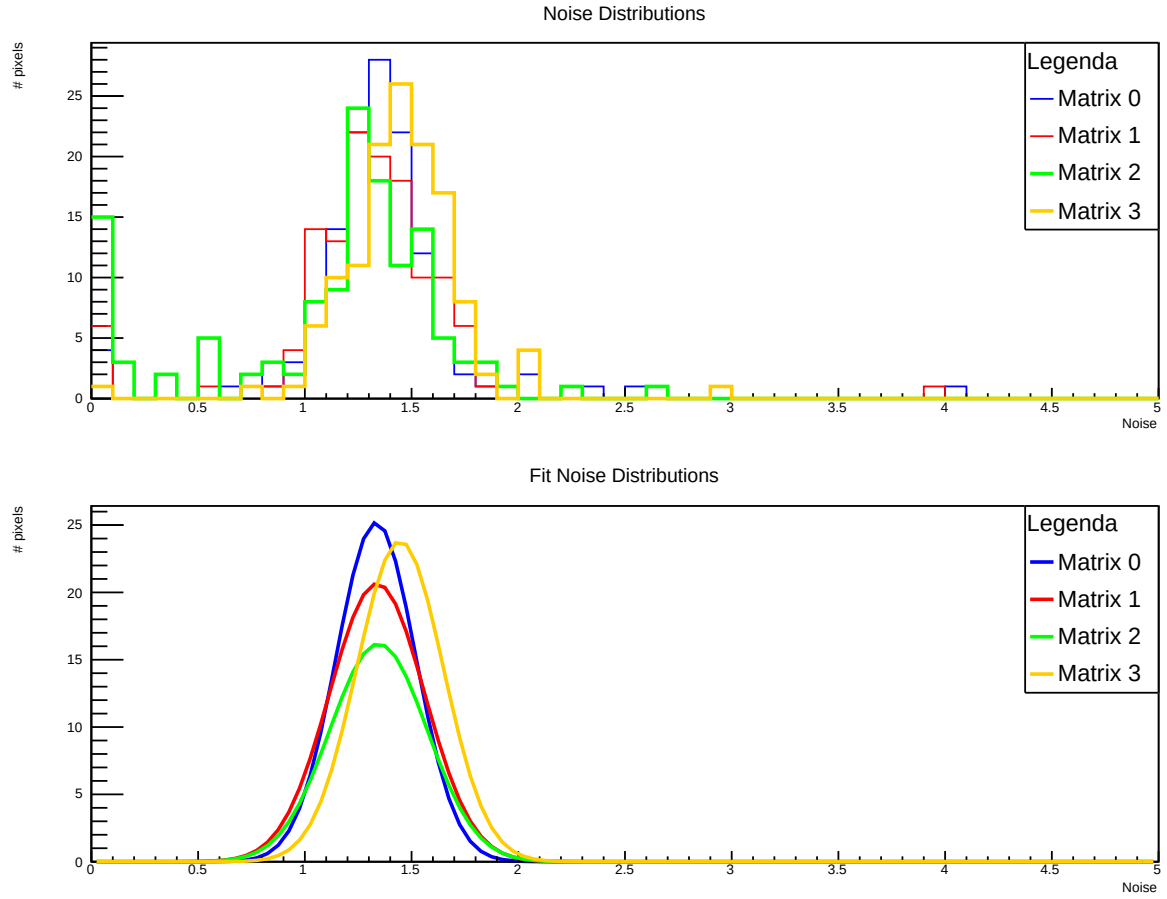

In the above distributions we can see that the noise distributions of the first dataset all have large overlapping regions. We can see in the table below that the mean noises don't differ a lot from each other though their spread has some differences. We saw in the pixel map and the threshold test of this dataset that matrix 2 had some clear anomalies and again we can see here that the first bin of the distribution is quite higher compared to the other matrices. This could again indicate faulty pixels or wrong fits of the error function. Furthermore, does matrix 0 have the most well defined and lowest noise of all the matrices.

Matrix	χ^2	ndf	χ^2/ndf	Prob(χ^2/ndf $\geq$ $\chi_0{}^2$/ndf)	Mean Noise
0	13.39	16	0.84	$69\% > P > 45\%$	1.33
1	14.12	13	1.09	$45\% > P > 27\%$	1.34
2	37.92	16	2.37	$5\% > P$	1.35
3	10.52	11	0.96	$64\% > P > 44\%$	1.45

Dataset 2
With this larger dataset we expect some more well defined noises of the pixels. Again the parameters are held the same as the previous dataset.

Figure 21: Dataset 2

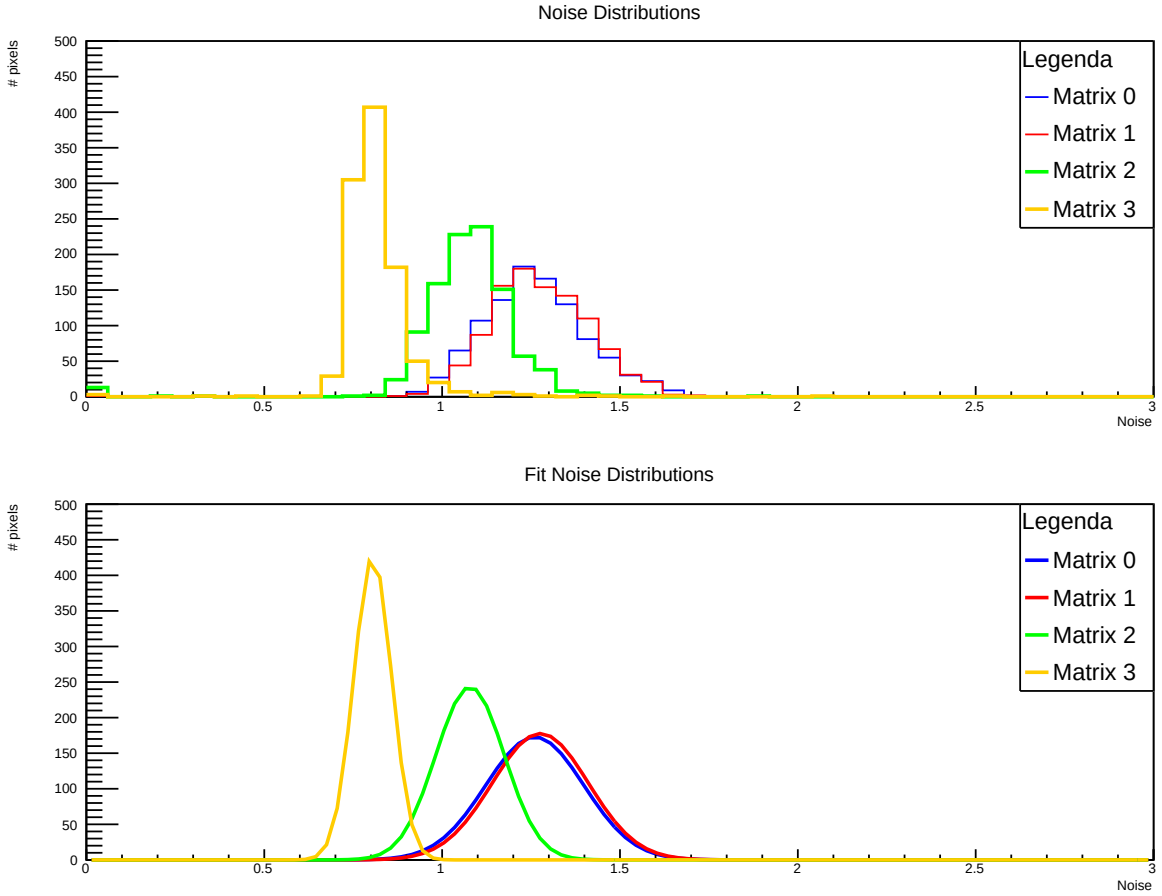

Above we can see that the noise distributions of this dataset clearly differentiate a lot more than the first dataset. First of all has matrix 3 changed from the pixel set with the highest mean noise to the one with the lowest mean noise. Also is its spread a lot smaller than all the other matrices which make it the matrix with the most well defined mean noise. Coincidentally does matrix 2 stay in the middle when regarding mean noise as well as spread of the noise and the matrices 0 and 1 have clearly the highest mean noise as can be seen in the distributions, fits and the table below. They also have the worst defined noise having the largest spread in their distribution compared to the other matrices. When we take a look overall we see that the mean noise however has been collectively lowered in this dataset though the probability of the reduced chi squared is again, just like with the threshold test of data set 2, worsened which indicates again a worse agreement with a Gaussian fit.

Matrix	χ^2	ndf	χ^2/ndf	Prob(χ^2/ndf $\geq {\chi_0}^2$/ndf)	Mean Noise
0	27.67	16	1.73	$5\% > P$	1.26
1	18.82	14	1.34	$27\% > P > 14\%$	1.28
2	44.46	16	2.78	$5\% > P$	1.08
3	76.52	16	4.78	$5\% > P$	0.80

Dataset 3
Again we used the heightened VCASN and thus lowered threshold to see in what ways it differs from the first but especially the second dataset.

Figure 22: Dataset 3

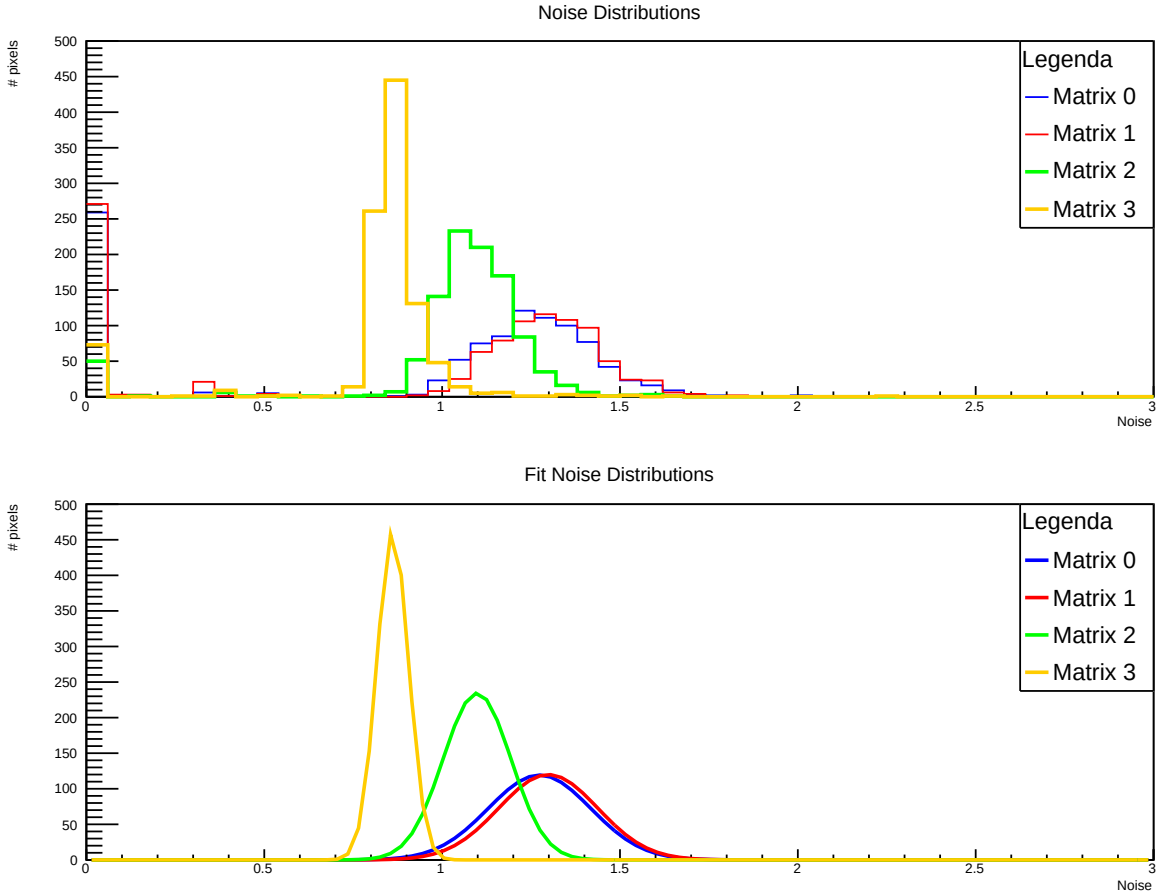

Just like with the threshold test we see that with matrix 0 and matrix 1 a heightened count of noises in the first bin is found. The relative position of the mean noises has however stayed the same and though they all were slightly higher than the noises of dataset 2 they still are lower then the mean noises of the distributions of the first dataset.

Matrix	χ^2	ndf	χ^2/ndf	Prob(χ^2/ndf $\geq$ $\chi_0{}^2$/ndf)	Mean Noise
0	304.06	24	12.67	$0.05\% > P$	1.27
1	322.70	21	15.37	$0.05\% > P$	1.30
2	91.04	19	4.79	$0.05\% > P$	1.10
3	165.01	20	8.25	$0.05\% > P$	0.86

4.4 Faulty Pixels

The previous distributions of the threshold and noise for the four different matrices have shown that a large amount of the pixels distribute them self in a near Gaussian way. However, in all of the datasets we saw that both threshold and noise values were found in the first bin. These represent either thresholds and noises of zero or a threshold and noise in the region of the first DACstep. Though the latter is highly unlikely when regarding the general distribution of the pixels we have to make sure which is the case. When we take a look at the way we determined the threshold it is possible that there are pixels which differ a lot from the distribution and simply have their threshold in the beginning region of the DACsteps in the threshold test. Another explanation could be that the fits are wrong and the threshold is wrongly determined. Noise however is determined by taking the derivative of the error fit which resembles the threshold test and this derived function is a Gaussian of which the sigma is the noise. This means that if the sigma should approach zero the Gaussian would take a form similar to a delta function and the threshold test that of a heaviside. This could be possible but noise this low is physically unlikely. A more plausible explanation is that the fit is again wrong in the way that the error fit is to steep when compared to the data points. We developed a piece of code that filtered out the threshold tests that have a very high reduced chi squared to see if there are extremely bad fitted error functions in the 3 data sets to see if there are some explanations for the occurrence of the heightened first bin count. A few examples were picked out but in appendix C you can find more of the faulty threshold tests. We will start with some fits from the first data set.

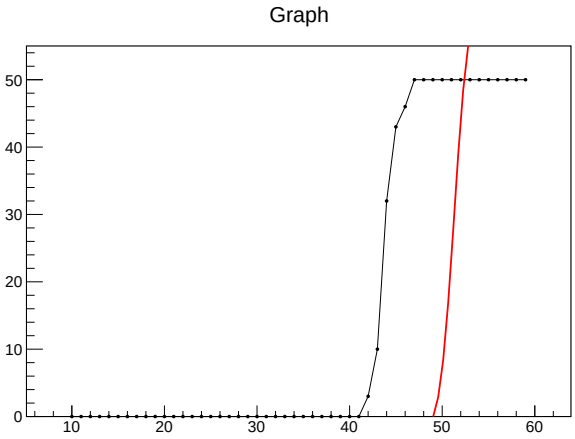

Figure 23: Example Fit nr. 1

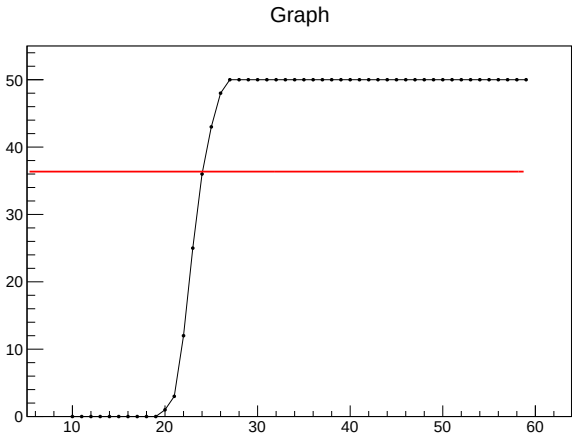

Figure 24: Example Fit nr. 2

The above figures are a clear example of a threshold test of which the fit is not well aligned with the data points. Though the first wrong fit does give a comparable noise since the slope of the fit does look similar to the slope of the data points it does however clearly illustrate that with a normal looking data set it can still give the wrong threshold and noise. The second figure also looks like a normal threshold test but again it depicts a very inadequate fit. If the derivative was taken from this fit to generate the gaussian needed for noise determination, it would give a zero-function which in its turn would result in a zero noise.

The previous two examples showed clearly that a good threshold test does not always give a well fit and therefore compromises the noise and threshold determination. Below are two other threshold tests and though they differ from the previous two examples all these data points and fits are still from the first data set.

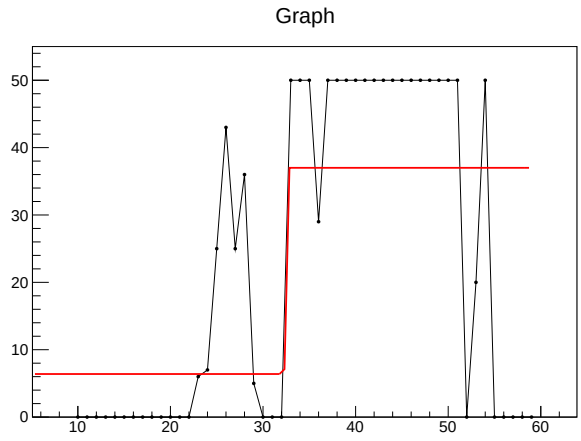

Figure 25: Example Fit nr. 3

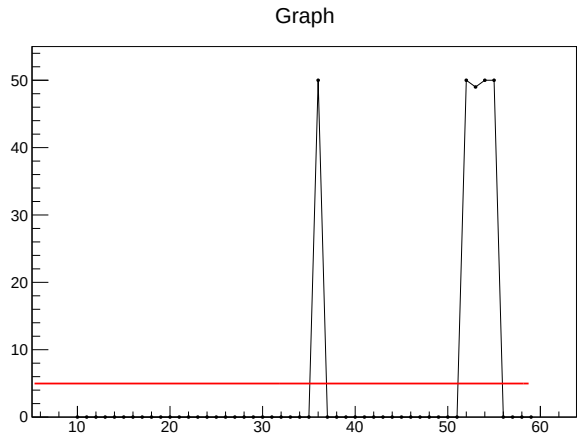

Figure 26: Example Fit nr. 4

The above figures clearly shows that instead of a clear threshold pattern in the data points some tests have a chaotic and unclear data point distribution. As of course one should expect does this not result in a good fit. The first figure gives a very steep heaviside-like function as predicted before which will result in an very small noise since the slope of the fit approaches infinity. The second data set lacks any slope at all and so if the fit is a flat function the noise will become zero as well.

The following example fits are from the second data set. Again we picked two which resembled the other fits the most and which had their data points or fit distributed in a abnormal way.

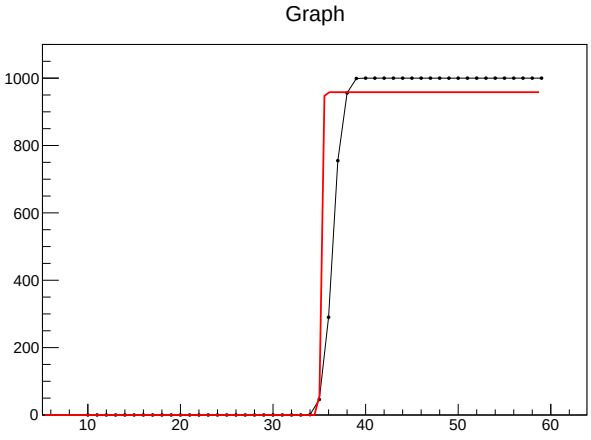

Figure 27: Example Fit nr. 5

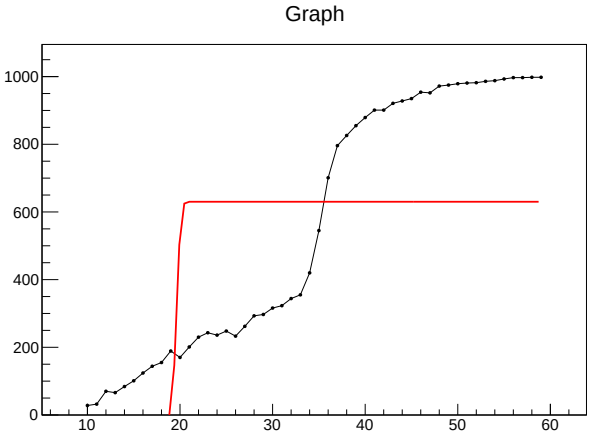

Figure 28: Example Fit nr. 6

In the left figure we see again a normal distributed set of data points which resemble a normal threshold test. However, the error function is again to steep fitted compared to the data points which results again in an abnormally low noise.

When we look at the right figure we see that this stands out from the other figures. In this case the data points are not chaotically ordered like in the previous two figures but neither are they smoothly and well distributed in an error function shape. And though a lot of the wrong fits are similar to example fit nr. 5, none of the wrong fits have a similar data point distribution like example fit nr. 6. Taking into account that we examined a very large set of pixels makes this an very odd occurrence.

The fits of the last data set have an even higher count of wrong fits. However, though this dataset has a larger amount of wrong fits they do seem to have similar flaws.

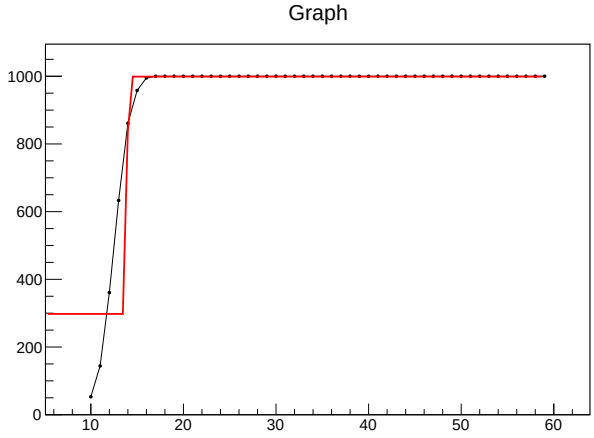

Figure 29: Example Fit nr. 7

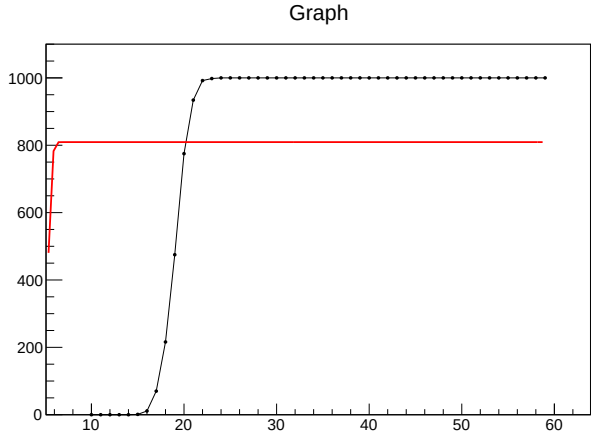

Figure 30: Example Fit nr. 8

As we can see the fits are again all to steep compared to the data points which results in the very low noise which was observed in the noise distributions. Furthermore, because the threshold is lowered in this data set we see that it is possible for a data set not to have enough data points to completely form an error function shape like in example fir nr. 7.

5 Conclusions

In the past sections we have showed that the theory of the Standard Model is far from complete. To fill up the gaps that are still left open in the theoretical field of particle physics experiments need to be performed to find the workings of the subatomic world. For ALICE the focus lies in the theory of the strong interactions, also know as Quantum Chromodynamics in which the collaboration has a well defined set of scientific goals. To achieve these goals regular maintenance and updates are needed of which in 2018-19 the next large upgrade is planned. One of the main goals of the upgrade is to renew the Inner Tracking System to improve spatial resolution, lower material budget, reduce power consumption, increase read-out capabilities and make the detector more accessible for regular maintenance. At the heart of the design of the ITS lies the Monolithic Active Pixel Sensor chip of which the ALPIDE architecture was the chosen chip design after researching several different architectures. We have tested the pALPIDe v2 chip which is a predecessor of the ALPIDE chip that is eventually being used in the ITS. In these paper we describe how it is possible to make mechanical and digital contact with the flex printed circuit on which chip was embedded. By the usage of a special made LVDS cable and a MOSAIC board connected via an ethernet cable to a computer one can run a threshold test on the pixels of the chip. With the statistical analysis framework Root we processed the threshold data from the 4 different matrices of the pixel chip and visualized them in plots and fits to determine the threshold and noise distribution of the different matrices. First of all we can conclude that in matrix 2 the data was influenced by something external. This is because the pixel map showed various pixels missing, the faulty pixels section showed chaotic and non-logical threshold tests and the other data sets showed none of these occurrences in their tests of matrix 2. It could be possible that the fluorescent lights in the room

of experiment had influence since the first data set was extracted without a cover over the pixel chip and the second and third did have a cover to shield them from the light. Furthermore can we conclude that when the amount of measurements per pixel per DACstep increases the Gaussian seems to be a less appropriate fit for the distribution of the thresholds and the noises. This is because the probability of the reduced chi squared of the distributions decreased a lot if the 50 and 1000 measurement data sets are compared. However, what the faulty pixels section showed is that the fits of the data points per pixel are not always well implemented which results in extremely low noise in the second and third data set. When we increased the parameter VCASN from 51 to 71 in the third data set we saw that the threshold is then lowered but resulted in some thresholds to become so low that the data points couldn't be fitted well. In all of the data sets we did not discover any pixels that always or never gave a hit, i.e. we did not find any dead pixels. This is of course promising when regarding the number of pixels tested and what the fake hit ratio should be on all the pixels.

6 Discussion

Though a very clear experimental framework has been set for testing ALPIDE chips there is still enough room for improvement. The first point of discussion is the experimental setup. We noticed that when performing the threshold test the dataset got altered and somewhat disturbed. In follow-up research the effect of light or other background radiation should be taken into account to see if this has any influence on the tests and if so, devise a cover that filters as much of the external influences as possible. Secondly, we developed tests for a single ALPIDE chip though the next step clearly should be to run a quality test on an array of chips. For this a new mechanical connection must be made but it is necessary since the chips all will be lastly tested in array form before they are build into the Inner Tracking System. The eventual read-out capabilities of the ITS will of course also be dependent on the electronics between the chips on the array and furthermore is it important to develop safe and delicate ways to transport the arrays of chips. Also the Root analysis that gave all the statistical information stated above has some points of improvement. As we saw with several threshold tests the data points that were well distributed in an error function way did not always have a correct fit. To improve this a more extensive differentiating of the fit parameters is needed to see if there is a more optimal way to fit the data points and decrease the amount of pixels with an abnormally low noise. This way noise and threshold both can be determined more accurately. Furthermore, we did not elaborate on how the parameters VCASN, ITHR and IDB in the data extraction program exactly influence the threshold. We knew roughly that increase of VCASN made a decrease in the threshold possible and increase ITHR and IDB a increase in threshold. A quantitative proportionality relation should be of great interest for testing the thresholds of ALPIDE chips since then one can show how well and accurate the thresholds can be set.

A Probabilities of Chi Squared

Table D. The percentage probability $Prob_d(\tilde{\chi}^2 \geq \tilde{\chi}_o^2)$ of obtaining a value of $\tilde{\chi}^2 \geq \tilde{\chi}_o^2$ in an experiment with d degrees of freedom, as a function of d and $\tilde{\chi}_o^2$. (Blanks indicate probabilities less than 0.05%.)

	$\tilde{\chi}_o^2$														
d	0	0.5	1.0	1.5	2.0	2.5	3.0	3.5	4.0	4.5	5.0	5.5	6.0	8.0	10.0
1	100	48	32	22	16	11	8.3	6.1	4.6	3.4	2.5	1.9	1.4	0.5	0.2
2	100	61	37	22	14	8.2	5.0	3.0	1.8	1.1	0.7	0.4	0.2		
3	100	68	39	21	11	5.8	2.9	1.5	0.7	0.4	0.2	0.1			
4	100	74	41	20	9.2	4.0	1.7	0.7	0.3	0.1	0.1				
5	100	78	42	19	7.5	2.9	1.0	0.4	0.1						

	0	0.2	0.4	0.6	0.8	1.0	1.2	1.4	1.6	1.8	2.0	2.2	2.4	2.6	2.8	3.0
1	100	65	53	44	37	32	27	24	21	18	16	14	12	11	9.4	8.3
2	100	82	67	55	45	37	30	25	20	17	14	11	9.1	7.4	6.1	5.0
3	100	90	75	61	49	39	31	24	19	14	11	8.6	6.6	5.0	3.8	2.9
4	100	94	81	66	52	41	31	23	17	13	9.2	6.6	4.8	3.4	2.4	1.7
5	100	96	85	70	55	42	31	22	16	11	7.5	5.1	3.5	2.3	1.6	1.0
6	100	98	88	73	57	42	30	21	14	9.5	6.2	4.0	2.5	1.6	1.0	0.6
7	100	99	90	76	59	43	30	20	13	8.2	5.1	3.1	1.9	1.1	0.7	0.4
8	100	99	92	78	60	43	29	19	12	7.2	4.2	2.4	1.4	0.8	0.4	0.2
9	100	99	94	80	62	44	29	18	11	6.3	3.5	1.9	1.0	0.5	0.3	0.1
10	100	100	95	82	63	44	29	17	10	5.5	2.9	1.5	0.8	0.4	0.2	0.1
11	100	100	96	83	64	44	28	16	9.1	4.8	2.4	1.2	0.6	0.3	0.1	0.1
12	100	100	96	84	65	45	28	16	8.4	4.2	2.0	0.9	0.4	0.2	0.1	
13	100	100	97	86	66	45	27	15	7.7	3.7	1.7	0.7	0.3	0.1	0.1	
14	100	100	98	87	67	45	27	14	7.1	3.3	1.4	0.6	0.2	0.1		
15	100	100	98	88	68	45	26	14	6.5	2.9	1.2	0.5	0.2	0.1		
16	100	100	98	89	69	45	26	13	6.0	2.5	1.0	0.4	0.1			
17	100	100	99	90	70	45	25	12	5.5	2.2	0.8	0.3	0.1			
18	100	100	99	90	70	46	25	12	5.1	2.0	0.7	0.2	0.1			
19	100	100	99	91	71	46	25	11	4.7	1.7	0.6	0.2	0.1			
20	100	100	99	92	72	46	24	11	4.3	1.5	0.5	0.1				
22	100	100	99	93	73	46	23	10	3.7	1.2	0.4	0.1				
24	100	100	100	94	74	46	23	9.2	3.2	0.9	0.3	0.1				
26	100	100	100	95	75	46	22	8.5	2.7	0.7	0.2					
28	100	100	100	95	76	46	21	7.8	2.3	0.6	0.1					
30	100	100	100	96	77	47	21	7.2	2.0	0.5	0.1					

The values in Table D were calculated from the integral

$$Prob_d(\tilde{\chi}^2 \geq \tilde{\chi}_o^2) = \frac{2}{2^{d/2}\Gamma(d/2)} \int_{\chi_o}^{\infty} x^{d-1} e^{-x^2/2} dx.$$

See, for example, E. M. Pugh and G. H. Winslow, *The Analysis of Physical Measurements* (Addison-Wesley, 1966), Section 12-5.

B FPC connections

Figure 32: FPC with which the connection is made

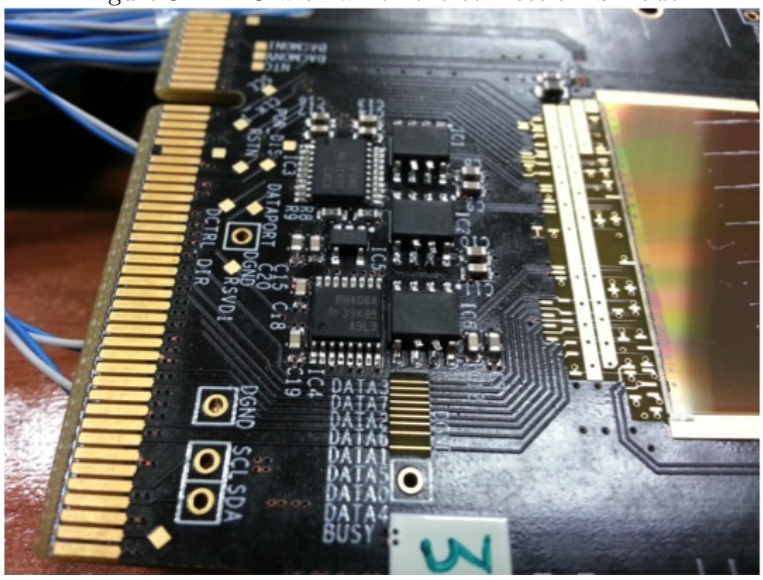

Figure 33: DATA, CNTR and CLK connection

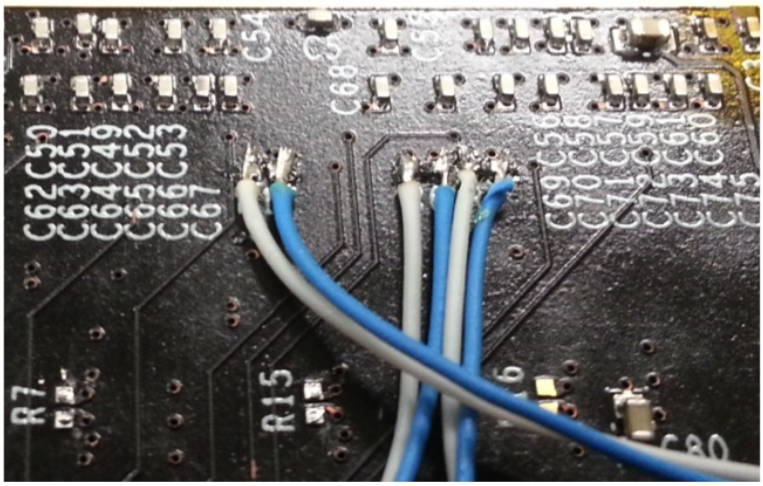

Figure 34: DGND and DVDD connection

Figure 35: AVDD and AGND connection

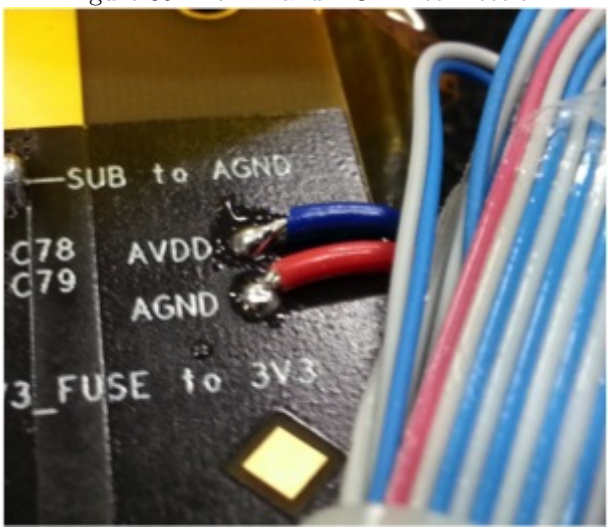

Figure 36: DGDN connection

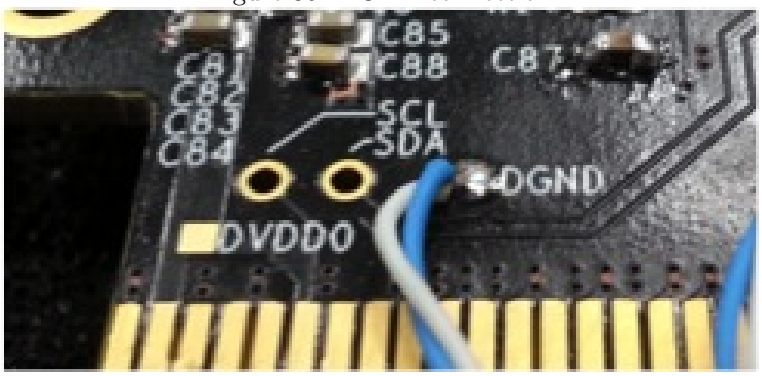

C Faulty Fits

Figure 37: Dataset 1

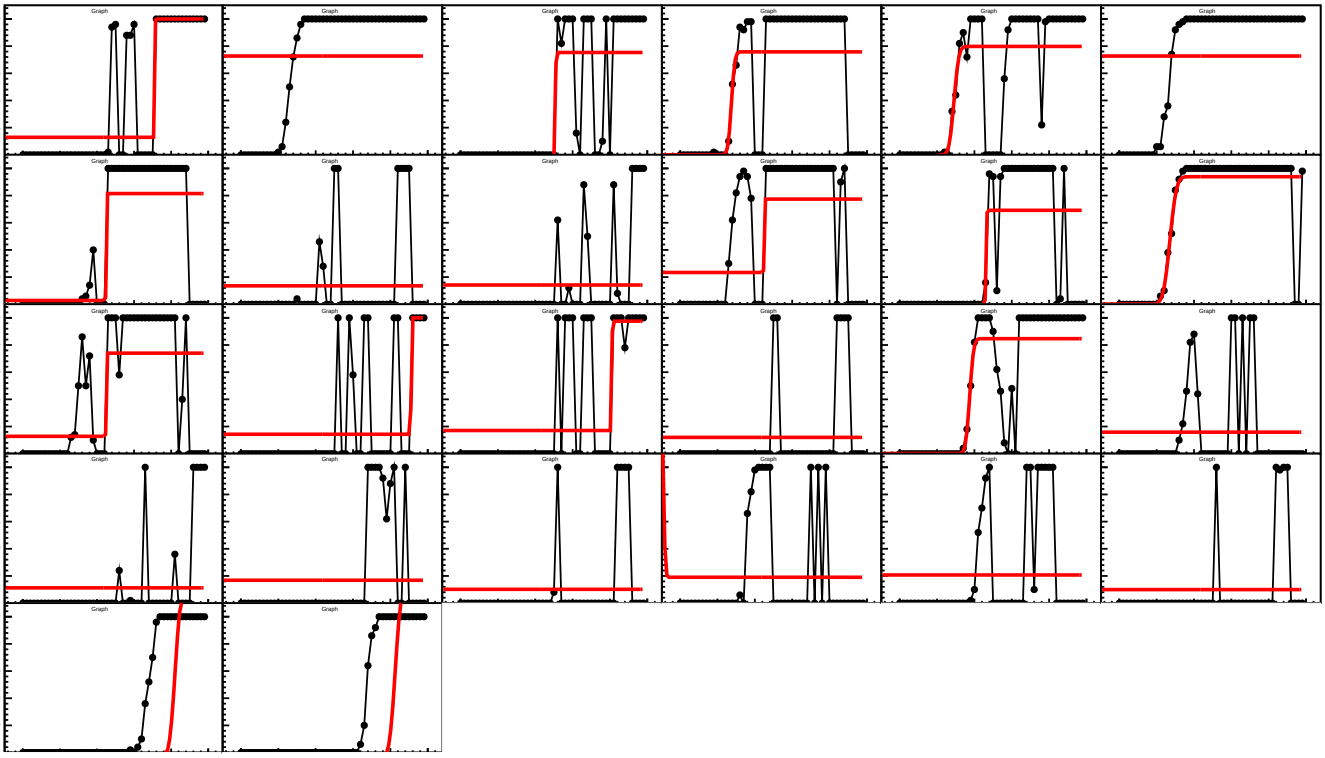

Figure 38: Dataset 2

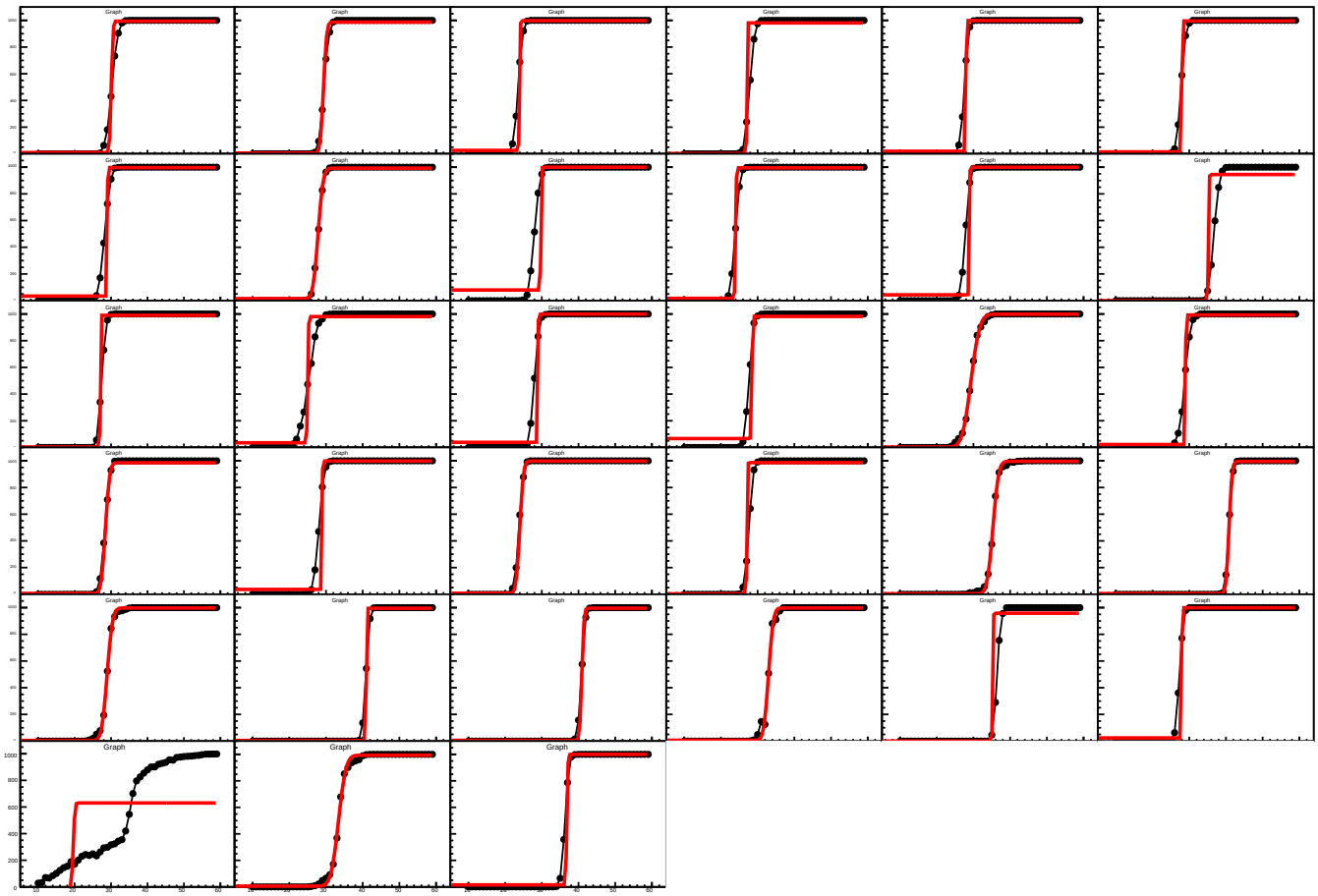

Figure 39: Dataset 3

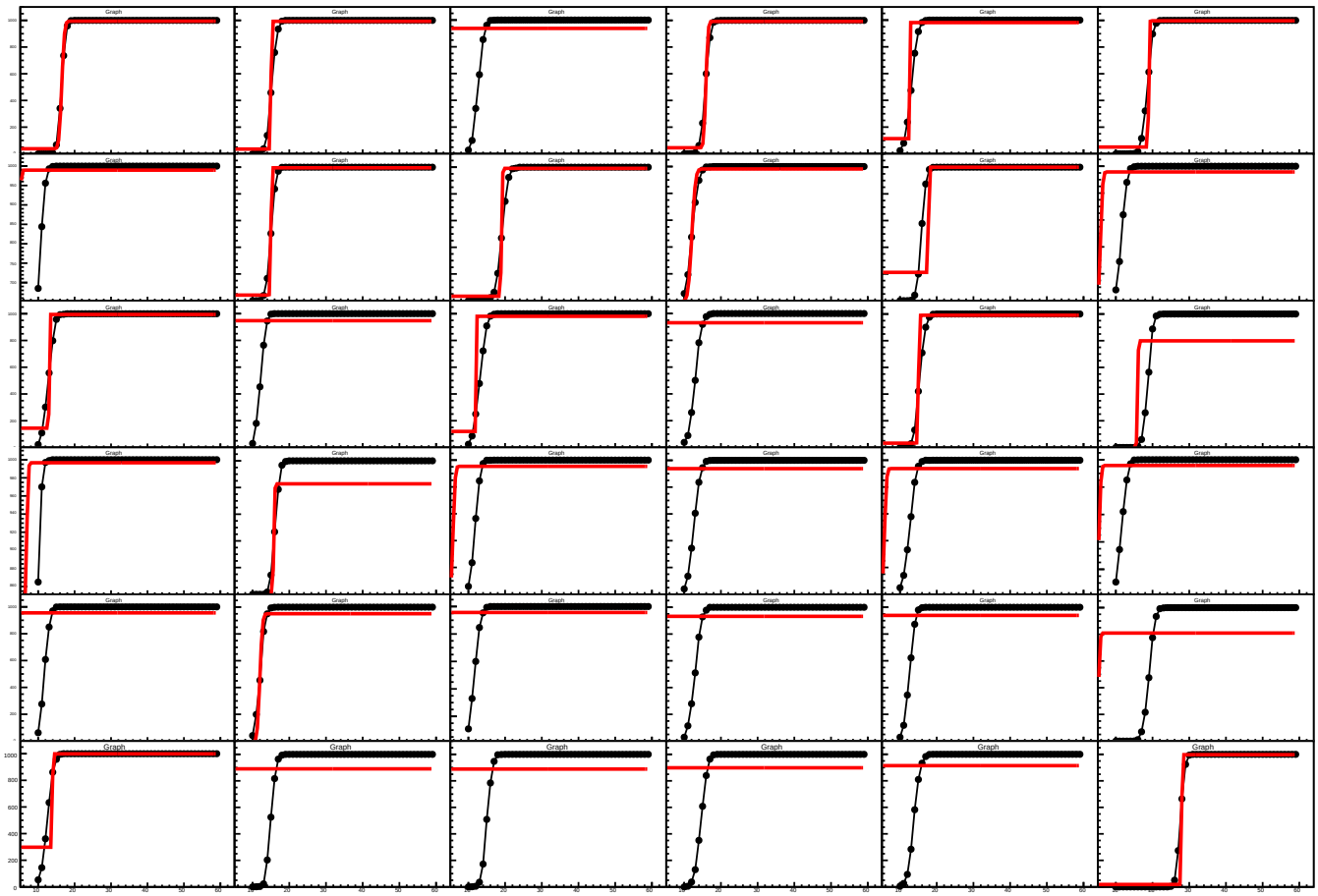

References

[1] Wikipedia, *The Standard Model*, https://en.wikipedia.org/wiki/Standard_Model

[2] Wikipedia, *Strong Interactions*, https://en.wikipedia.org/wiki/Strong_interaction

[3] F. Wilczek, *QCD Made Simple*, http://frankwilczek.com/Wilczek_Easy_Pieces/298_QCD_Made_Simple.pdf

[4] Wikipedia, *Quantum chromodynamics*, https://en.wikipedia.org/wiki/Quantum_chromodynamics

[5] F. Muheim, *QCD Lecture*, Lecture Slides University of Edinburgh, http://www2.ph.ed.ac.uk/ muheim/teaching/np3/lect-qcd.pdf

[6] Physics Central, *Quark Gluon Plasma*, http://physicscentral.com/explore/action/gluon.cfm

[7] Wikipedia, *ALICE: A Large Ion Collider Experiment*, https://en.wikipedia.org/wiki/ALICE:_A_Large_Ion_Collider_Experiment

[8] Wikipedia, *Quark Gluon Plasma*, https://en.wikipedia.org/wiki/Quark-gluon_plasma

[9] P. Kuijer, *Personal Communication*, (2015)

[10] CERN Courier, *ALICE gets with the flow*, http://cerncourier.com/cws/article/cern/45436

[11] B. Abelev *et al.* [The ALICE Collaboration], *Conceptual Design Report for the Upgrade of the ALICE Inner Tracking System*, Tech. rep. CERN-LHCC-2012-005 (2012)

[12] N. van der Kolk [Nikhef], *A study of elliptic flow and nonflow in proton-proton collisions in ALICE*, Ph.D. Thesis University Utrecht (2012)

[13] B.S. Nilsen [The ALICE Collaboration], *Heavy-flavor production in LHC pp interactions using the ALICE detector*, Nucl. Phys. Proc. Suppl. 233 (2013), arXiv:1210.7847 [hep-ex]

[14] Peter Petreczky, *Spectral function in Quark Gluon Plasma*, Lecture Slides National Laboratory Brookhaven (2014), https://www.olcf.ornl.gov/wp-content/uploads/2013/02/Petreczky_P_LQCD1.pdf

[15] F. Carminati *et al.* [The ALICE Collaboration], *Physical Performance Report Volume I for the Upgrade of the ALICE Inner Tracking System*, J. Phys. G: Nucl. Part. Phys. 30 (2004), doi:10.1088/0954-3899/30/11/001

[16] K. Aamodt *et al.* [The ALICE Collaboration], *The ALICE experiment at the CERN LHC*, (2008)

[17] B. Abelev, *et al.* [The ALICE Collaboration], *Technical Design Rapport for the Upgrade of the ALICE Inner Tracking System*, J. Phys. G: Nucl. Part. Phys. **41** (2014) 087002, doi:10.1088/0954-3899/41/8/087002

[18] B. Abelev, *et al.* [The ALICE Collaboration], *Technical Design Rapport for the Upgrade of the ALICE Inner Tracking System*, J. Phys. G: Nucl. Part. Phys. **41** (2013) 087002, doi:10.1088/0954-3899/41/8/087002

[19] D. Silvermyr [The ALICE Collaboration], *ALICE Upgrade Program*, ORNL Slides (2014)

[20] F. Reidt [The ALICE Collaboration], *Upgrade of the ALICE Inner Tracking System*, Proceedings of Science, (2015), arXiv:1411.1802v2

[21] P. Yang *et al.* [The ALICE Collaboration], *ALPIDE Design*, ALICE, MFT and 02 Asian Workshop Slides (2015)

[22] ALICE ITS ALPIDE development team, *ALPIDE-3 Operations Manual - DRAFT*, (2015)

[23] J.D. Schipper, *Personal Communication*, (2015)

[24] M. Reil [The ALICE Collaboration], *PALPIDE Testing*, ALICE Plenary Meeting Slides (2014)

[25] J.R. Taylor, *Error Analysis*, (1997), p. 292-293